Manipulation and Characterisation of Two Photon Spectral Correlation States in Nonlinear Devices

By

IMAN JIZAN

A thesis submitted in fulfilment of the requirements for the degree of Masters of Science

School of Physics
University of Sydney
Australia

MARCH 2016

Declaration of Originality

I hereby declare that this thesis to the best of my knowledge contains no materials of work published or written by another person, except where duly acknowledged in the text. This thesis has not been previously submitted for a degree at the University of Sydney or any other any institution.

I declare this thesis to be a product of my own work, unless stated otherwise.

Iman Jizan

ACKNOWLEDGEMENTS

Studying for my Masters has been the experience of a lifetime, one that has allowed me to work with some wonderful and intelligent people of physics and quantum photonics. As such there are quite a few people I need to thank for their help and support during my studies.

The first and foremost thanks must go to my supervisor, Prof. Ben Eggleton, for welcoming me into CUDOS and providing me with such an excellent research environment for optics and photonics. I will always be grateful for his support, advice and encouragement that started when I first enrolled in Honours three years ago.

Many, many thanks to my co-supervisor Dr. Chunle Xiong for his guidance, support and insightful discussions throughout the years. Thank you for being a great co-supervisor and for patiently teaching me nonlinear photonics when I needed help. I have learnt so much while working with you.

I would like to thank Prof. Mike Steel and especially Dr. Luke Helt in Macquarie University for not only their advice and encouragements, but also going out of their way on many occasions to explain nonlinear and quantum photonics to me when I first started.

Thank you to Dr. Alex Clark for being a great co-supervisor during Honours and always challenging me and encouraging me to do better.

To Dr. Bryn Bell, I have wholeheartedly enjoyed our interesting discussions of quantum photonics. Thank you for being an awesome lab partner during my last few months in CUDOS.

To my past and present office mates, thank you for the constant laughs, fun discussions and encouragements in my time of need. Your friendship means more to me than you realise.

I would finally like to thank to my family for always being there for me and instilling me with the desire to follow my dreams. I could not not have achieved so much if it was not for their unconditional support that they have provided me throughout my life.

Abstract

In quantum photonics, the requirement for photon pairs with specific quantum states has led to a demand for a fast, high resolution and accurate characterisation of photon pair sources. However, current quantum methods of characterisation suffer from limited accuracy and resolution, and only consist of intensity measurements that prevent access to phase-sensitive measurement photon pairs. A promising tool that addresses these challenges, uses the classical analogue of nonlinear processes to stimulate photon generation, yielding much higher count rates that allows for a higher resolution and accurate photon pair source characterisation. Furthermore, this classical measurement allows for an innovative method to perform full phase-sensitive quantum tomography of photon pair sources that was previous thought to be experimentally challenging to obtain.

This thesis examines and compares the quantum and classical method of characterisation of spectral correlations in $\chi^{(3)}$ nonlinear devices; namely two integrated silicon nanowires, and a highly nonlinear fibre. In the first study, we use stimulated nonlinear process to confirm the speed-up of characterisation of photon pairs and demonstrate that additional resolution is gained when compared to the traditional coincidence measurements with no increase in measurement time. By applying this technique with phase-sensitive amplification to another identical silicon nanowire, the first phase sensitive measurements are presented showing details that are otherwise hidden in traditional intensity measurements. Furthermore, phase-sensitive measurement of a highly nonlinear fibre shows that phase-sensitive measurements have excellent sensitivity to small features when compared to the traditional intensity measurements.

List of Abbreviations

KLM	Knill-Laflamme-Milburn
CNOT	quantum NOT gate
FWM	four-wave mixing
PDC	parametric down conversion
CAR	coincidence to accidental ratio
TIA	time interval analyser
PPLN	Quantum NOT Gate
HNLF	highly nonlinear fibre
CMOS	complementary metal-oxide-semiconductor
JSI	joint spectral intensity
JSA	joint spectral amplitude
K	Schmidt number
SNLB	Schmidt number lower bound
SVD	singular value decomposition
FWHM	full width at half maximum
GVD	group velocity dispersion
DFG	difference frequency generation
OSA	optical spectrum analyser
SiNW	silicon nanowire
SNR	signal to noise ratio
SOI	silicon-on-insulator
PC	polarisation controller
ISO	isolator
ATT	attenuator

TBPF	tunable band-pass filter
PM	power meter
EDFA	erbium doped fibre amplifier
IM	intensity modulator
PG	pulse generator
AWG	arrayed waveguide grating
LCoSWS	liquid-crystal-on-silicon dynamically tunable filter
SSPD	superconducting single photon detector
CW	continues wave
PSA	phase sensitive amplification

TABLE OF CONTENTS

Page

List of Tables **xi**

List of Figures **xiii**

1 Introduction **1**

2 Background of Photonics **3**

2.1 Quantum Information 3

2.1.1 Single Photons as Quantum Systems 5

2.1.2 Quantum interference of Single Photons 6

2.2 Nonlinear Optics 8

2.2.1 Generation of Single Photons 8

2.2.2 Photon Statistics and Coincidences 10

2.2.3 A Brief History of Nonlinear Optics 12

2.2.4 Four-Wave Mixing 13

2.2.5 Nonlinear Devices 15

2.3 Quantum Entanglement 16

2.3.1 Spectral Correlation 16

2.3.2 Joint Spectral Intensity and the Schmidt Number 17

3 Joint Spectral Intensity **21**

3.1 Theoretical Model 22

3.1.1 Pump Envelope Function 22

3.1.2 Phase-Matching Profile 22

3.1.3 Joint Spectral Intensity 24

3.2 Previous Quantum Measurement Schemes 25

3.3 An Alternative to Quantum Measurements 29

3.3.1 The Nonlinear Device 30
3.3.2 Quantum Measurements 31
3.3.3 Stimulated Measurements 33
3.4 Joint Spectral Intensity Results 35
3.4.1 Conclusions 39

4 Phase-Sensitive Joint Spectral Amplitude Measurement 41
4.1 The Joint Spectral Amplitude 42
4.2 Measurement of the Joint Spectral Amplitude 44
4.3 The Experimental Setup 46
4.4 Joint Spectral Intensity Results 48
4.4.1 Silicon Nanowire: Un-Chirped Pump 48
4.4.2 Silicon Nanowire: Chirped Pump 49
4.4.3 Highly Nonlinear Fibre: Un-Chirped Pump 51
4.5 Conclusions 52

5 Summary and Conclusions 53

A Appendix: Publication List 55

Bibliography 57

List of Tables

Table **Page**

2.1 Truth table of a linear CNOT gate, where C and T are the control and target qubits respectively. 6

2.2 A summary of current methods used to characterise the spectral correlations of photon-pairs generated via spontaneous FWM and spontaneous PDC. . . . 18

3.1 Theoretically extracted SNLBs, $\tilde{K}$, for a 40 by 40, 157 by 157 and ideal JSIs, for the 270 ps 100 MHz and 10 ps 50 MHz laser pump pulses. 36

List of Figures

Figure **Page**

2.1 An example of a multi-input digital gate that produces a single output. 5

2.2 The four possible paths photons can take when entering a 50% reflective mirror (50:50 beam splitter). 7

2.3 Atom-like source that emits a single photon when the atom decays from its excited to its ground state. 9

2.4 Schematic illustration of a single photon source by the attenuation of a laser source. 9

2.5 Schematic illustration of photon pair generation in a nonlinear medium, allowing for the heralding of the partner photon. 10

2.6 A typical CAR histogram is shown. Inset shows single photon pairs reaching a pair of single photon detectors. Photon-pair arrival times are analysed using a TIA which are then used in a CAR histogram. 11

2.7 Illustration of (a) classically stimulated FWM process and (b) spontaneous FWM. 14

2.8 A typical (a) JSI measurement with the centre pump frequency highlighted and (b) JSI measurement for no correlation (K = 1) and high correlations (K»1) between the signal and idler photon pairs. 19

3.1 Normalised theoretically calculated model of the pump function, for a typical pump pulse width of 10 ps. 23

3.2 The normalised theoretically calculated model of the phase matching function for a waveguide with a $k_0 = 9.63 \times 10^6$ $v_p = 7.02 \times 10^7$ m/s and $GVD = -6.03 \times 10^{-25}$ s^2/m 25

3.3 The final normalised theoretically calculated model of the JSI for a pump and phase matching functions given in the previous sub-sections. 26

3.4 The conventional approach for a JSI measurement consisting of a highly dispersive fibre that temporally separates the signal and idler photons. The stream of signal and idler photons are detected and time tagged using a TIA to build a JSI plot. 26
3.5 Another approach for a JSI measurement that uses tunable optical band pass filter to spatially separate the signal and idler photons that are generated via the nonlinear device. To measure the JSI, the wavelength of the tunable band pass filter needs to scan the FWM bandwidth of the nonlinear device. 27
3.6 Two coincidence measured JSIs of photon pairs in the telecommunication band using (a) temporal dispersion method for spontaneous PDC process with resolution of 1.2 nm and (b) spatial separation method for spontaneous FWM process with a resolution of 80 pm. 28
3.7 Schematics of (a) 3 mm Buried SiNW, the cross-sectional dimensions and (c) the simulated $|\mathbf{B}|^2$ energy density of the fundamental TE mode. 30
3.8 The experimental setup for (a) 10 ps, 50 MHz pump and (b)270 ps, 100 MHz pump. See text for the full details of experimental setup. 32
3.9 Schematics of the experimental setup for coincidence measurement of the JSI using the spatial separation method. See text for details. 33
3.10 The seed laser used the second channel of an ECDL, set to TE polarisation using a PC and filtered clean using TBPF before being combined with the 10 ps or 270 ps laser source to stimulate FWM. 34
3.11 The experimental setup for measurement of idler photons generated via stimulated FWM using (a) the spatial separation method and (b) an OSA. See text for details. 34
3.12 The scaled theoretically-calculated model for (a) the 270 ps and (b) 10 ps pump laser pulses, with dashed box representing the measured region. 35
3.13 The results of the six JSI measurements, for (a) the 270 ps and (b) 10 ps pump laser pulses: (i) photon pair coincidence measurement, (ii) stimulated FWM singles-based measurement and (iii) stimulated FWM OSA measurement. The brightest pixel in each plot (Max of the colour bar) corresponds to: (a)(i) 105 coincidences, (b)(i) 105 coincidences, (a)(ii) 318,720 counts, (b)(ii) 182,210 counts, (a)(iii) 1716.7 nW/10 GHz, and (b)(iii) 464.1 nW/10 GHz. These maxima all have Poissonian error except those for (a)(iii) and (b)(iii) which have an inherent error from the OSA. SNLBs are shown for each plot with errors calculated from Monte Carlo simulations. 37

4.1 Schematics of a homodyne detection setup where the output signal is split and interfered with itself. 42
4.2 A schematic drawing of a homodyne detection setup where the generated field via stimulated FWM is combined with a local oscillator before detection with a photodetector. 44
4.3 An illustration of PSA where the generated field via stimulated FWM is interfered with a reference field resulting in constructive or deconstructive interference as the phase of the seed field is varied. 45
4.4 Schematics of the experimental setups of JSA measurement for 6 mm silicon nanowire (SiNW) and a 200 m highly nonlinear fiber (HNLF). See text for detailed description. 46
4.5 The (a) measured and (b) theoretically modelled plots of (i) JSIs, and normalised plots of (ii) real and (iii) imaginary parts of the JSA of SiNW for a frequency un-chirped pump. 49
4.6 The (a) measured and (b) theoretically modelled plots of (i) JSIs, and normalised plots of (ii) real and (iii) imaginary parts of the JSA of SiNW for a frequency chirped pump. 50
4.7 The (a) measured and (b) theoretically modelled plots of (i) JSIs, and normalised plots of (ii) real and (iii) imaginary parts of the JSA of HNLF for a frequency un-chirped pump. 51

CHAPTER 1

INTRODUCTION

We live in an age where information is a vital resource and our society and economy is constantly shaped by computation and communication as we rely on faster and faster information processing. Quantum information is an exciting field that promises to solve some computational tasks and implement communication protocols that are not possible with current classical computers and communication systems [1–3]. The emergence of quantum information technologies in recent years has therefore led to an ever-growing field that combines the non-classical behaviour of physics with real-world technological applications. This system consisted of exploiting quantum particles such as electrons, ions or photons that exhibit non-intuitive behaviours of quantum mechanics, such as superposition and entanglement, for use in quantum information technologies. Photons do not strongly interact with matter or with one another and therefore are well isolated quantum systems that can exhibit stable superposition and entanglement even at room temperature compared to other quantum systems. Additionally, they are the only viable choice for quantum communications and can provide a natural integration between quantum computation and quantum communication.

Prior to early 2000s, optical quantum experiments were performed using table-top and bulky optical elements that used nonlinear optical processes to provide optical switching when two or more optical signals are combined [4]. It was soon realised however, that this approach would become easily unstable and unwieldy to scale up. Fortunately a solution was proposed in 2001 that uses single photon sources, linear optical components and single photon detectors for optical switching in the single photon

regime [5]. This approach introduced the new field of quantum photonics that aims to solve many of the challenges of traditional optical quantum computing experiments.

The ability to prepare and precisely control the state of single photons is critical to the advancement of quantum photonics as we require specific photons states for different tasks such as quantum computing where non-entangled photons states are required to exhibit quantum interference. As we are constantly moving towards more integrated and complex quantum photonic platforms, this has created a demand for fast, high resolution and accurate source characterisation of single photons.

This thesis presents significant progress towards the manipulation and characterisation of photon pairs generated in nonlinear media. Chapter 2 starts with the introduction and background of quantum information science and the use of single photons as quantum systems. The mathematics underlying the characterisation of spectral entanglement which will be used at several points in the later chapters is also introduced. Chapter 3 begins with traditional methods of characterisation of photon pairs using intensity based quantum measurements. To address some of the limitations imposed by the quantum measurements, a new method of photon pair source characterisation that uses classical stimulated processes is then introduced. In chapter 4, this classical measurement combined with a novel method is used to perform phase-sensitive measurements of photon pair sources, a measurement that was previously thought to be experimentally inaccessible. The experimental investigation of characterisation of photon pairs is crucial to the future development of complex sources of photon pair states for use in future quantum photonic technologies.

CHAPTER 2

BACKGROUND OF PHOTONICS

Quantum mechanics provides an elegant method for the description of the motion and interaction of subatomic particles. The non-intuitive behaviour of quantum mechanics has had a transforming effect in the field of communication, computation and metrology where it enables us to go beyond the realm of classical limits. After a brief introduction to quantum information, this chapter contains:

- Analysis of single photons as a quantum system and application of single photons in quantum photonics.
- Introduction to nonlinear optics and exploration of the current methods used to generate single photons.
- In depth analysis of the current method used to characterise and quantify the degree of spectral correlations of photon pairs generated via nonlinear devices.

2.1 Quantum Information

Quantum mechanics, since its development and maturity into its current form in the late 1920s, is among the most successful and mysterious of scientific theories. Quantum mechanics portrays a world that is fundamentally probabilistic, where single fundamental entities can be at two places at the same time, and also where two fundamental entities that are light years apart can be instantaneously linked. It is important to note that

the two fundamental entities cannot send or receive information faster than light and no local causality is broken. In the decades following the 1920s, physicists have successfully applied quantum mechanics to not only the understanding of the fundamental physical laws but also to the technological advancement of science. However, only in the last decades, the unintuitive behaviour of quantum mechanics has been applied to computing and communication [6–8]. In quantum computing, powerful computations can be performed for specific tasks enabled by the superposition of quantum systems, while quantum communication takes advantage of the no-cloning theorem - where we cannot clone an unknown quantum state without destroying it.

In quantum information, one of the key fundamental units is the qubit, the quantum analogue of the classical bit that can be in a 0 or a 1 state, with the corresponding wavefunction written in Dirac's notation as $|0\rangle$ and $|1\rangle$. In quantum information, a qubit is commonly expressed as a superposition state of both states at the same time, represented by

$$|\psi\rangle = \alpha|0\rangle + \beta|1\rangle \tag{2.1}$$

where α and β are the probability amplitudes of the qubit such that a measurement of $|\psi\rangle$ will give $|0\rangle$ with probability of $|\alpha|^2$ or $|1\rangle$ with probability $|\beta|^2$. As such superposition state is normalised with total amplitude probability of $|\alpha|^2 + |\beta|^2 = 1$. As the amplitude probability can be complex, many interesting effects such as quantum interference can take place.

In quantum information, there are many types of quantum systems whose qubit degree of freedom can be used in quantum information science. However there exists a few crucial criteria that these quantum systems must have in order to be successful for use in quantum information technologies. Generally the criteria requires the quantum system to contain well characterised quibits, long coherence times after relevant operations and relatively easy measurement ability of specific quibits. Currently there exists many quantum systems that meet, to a certain extend, these criteria. Examples of such platforms include trapped ions [9], electrons [10], superconducting junctions [11] and photons [12]. However, each platform has its own unique technical challenges and advantage.

2.1.1 Single Photons as Quantum Systems

In recent years, photons have emerged as potential quantum systems that can be used for long-distance quantum communication and quantum computation. The biggest advantage of photons is that photons do not interact strongly with matter and thus are a prime candidate for transmitting photons through existing optical fibre communication networks with low loss for quantum communication. However, this can also be a disadvantage where we require photons to interact with each other for use in quantum information technologies. More specifically, strong interaction between photons is required to perform gate operations. This therefore causes major difficulty and challenges in the implementation of optical gates in optical circuits in quantum optical technologies.

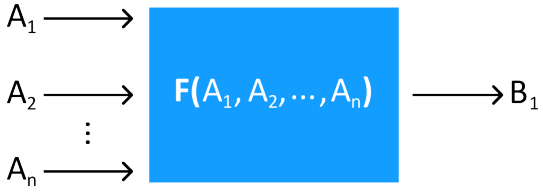

FIGURE 2.1. An example of a multi-input digital gate that produces a single output.

In conventional computing, classical logic gates are used for digital circuits where they switch the output state depending on the input states of the system (see Fig. 2.1). This system uses voltages that has two nominal values representing logic 0 and logic 1. In optics however, the property of weak interaction between photons becomes a large problem for qubit computation.

In 1995, a solution was purposed to use nonlinear optics to allows for photon-photon interaction [13]. This scheme requires two beams of photons, a control and the target beam, to interact nonlinearly such that the control beam induces a π phase shift in the target beam. However in the single photon regime, it is found to be extremely difficult task to induce a π phase shift by a single photon using the classical scheme of nonlinear optics [14, 15].

Fortunately, a breakthrough scheme was proposed in 2001 that allows for efficient photon-photon interaction using linear optical components [5]. This proposal is currently known as the Knill-Laflamme-Milburn (KLM) scheme that is based on two single photons to interact in a beam splitter to induce a π phase shift in the target photon, without the need for nonlinear optics. This interaction in the beam splitter leads to quantum interference that is critical for the development of quantum computation and processing

Input		Output	
C	T	C	T
$\|0\rangle$	$\|0\rangle$	$\|0\rangle$	$\|0\rangle$
$\|0\rangle$	$\|1\rangle$	$\|0\rangle$	$\|1\rangle$
$\|1\rangle$	$\|0\rangle$	$\|1\rangle$	$\|1\rangle$
$\|1\rangle$	$\|1\rangle$	$\|1\rangle$	$\|0\rangle$

TABLE 2.1. Truth table of a linear CNOT gate, where C and T are the control and target qubits respectively.

that use qubit gate operation based on single photons. This scheme has led to the birth of quantum photonics and thus the development of radical new ways to manipulate photon states.

In quantum photonics, the quantum analogue of the classical gate, the quantum gate, is the building block for quantum circuits. An example of a quantum gate is the controlled NOT (CNOT) gate that is essential for the construction of a quantum computer. The CNOT gate operates with two input qubits named the controlled and the target (see Table. 2.1.1). The CNOT gate flips the target qubit if and only if the controlled qubit is $|1\rangle$. This CNOT gate is inherently useful for universal schemes of quantum information processing that requires two quibit gates [16].

2.1.2 Quantum interference of Single Photons

The non-classical interaction between photons is the key to quantum gates and thus quantum photonic technologies. However, for this interaction to occur, the photons require to be in specific quantum states. In general, it is possible to describe a photon in a quantum system by their degrees of freedom given by

$$|\Psi\rangle = |n, \lambda, P, T, S\rangle\,, \tag{2.2}$$

where n is the number of photons, λ is the photon's central wavelength, P is the photon polarisation, T is the temporal and S is the spatial mode of the photons. If we have two photons with identical quantum states as Eq. 2.2, the photons are indistinguishable and can therefore successfully quantum interfere with each other.

The first quantum interference was performed by Hong, Ou and Mandel in 1987 [17]. This ground-breaking experiment consisted of injecting two photons into each input path of a 50:50 beam splitter, which is a mirror that has a transitivity and reflectivity of 50%. Referring to Figure 2.2, when inputting two distinguishable photons that have

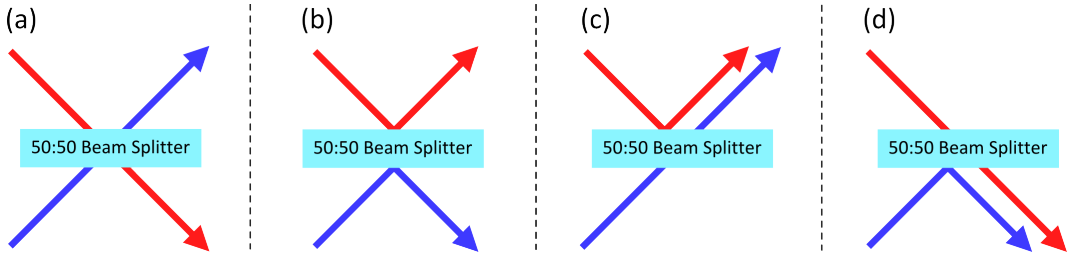

FIGURE 2.2. The four possible paths photons can take when entering a 50 % reflective mirror (50:50 beam splitter).

different wavelengths, there exists four possible paths that the photons can take; both photons can transmit (Fig. 2.2 (a)), both can reflect (Fig. 2.2 (b)) or one of the photons can transmit and the other to reflect ((Fig. 2.2 (c) and (d)). If we place two photon detector that are strategically in each of the 50:50 beam splitter output, the probability of obtaining a coincidence between the two detectors can be determined. If the two photons that enter the 50:50 beam splitter are distinguishable (as shown in Figure 2.2), the probability of obtaining a coincidence is given by the sum of the probability of both photons transmitting, and both photons reflecting. The probability of a coincidence is therefore

$$P_{Coincidence} = P_t + P_r \tag{2.3}$$

where P_t and P_r are the probabilities of both photons transmitting and reflecting respectively. Since the transmitance and reflectivity of such beam splitter is 50%, Eq. 2.3 can be written as

$$P_{Coincidence} = |\frac{1}{\sqrt{2}} \cdot \frac{1}{\sqrt{2}}|^2 + |\frac{1}{\sqrt{2}} \cdot \frac{1}{\sqrt{2}}|^2 = \frac{1}{2}. \tag{2.4}$$

This calculation indicates that when two distinguishable photons enter a 50:50 beam splitter, we expect a coincidence between the two detectors 50% of the time.

Now if we consider quantum mechanics, where two photons can poses the exact same quantum states and input these two photons into the same 50:50 beam splitter, a different coincidence probability is calculated. Although the probability of each photon to transmit through the 50:50 beam splitter is the same for distinguishable photons (the first term in Eq. 2.5), in the reflected case each photon experiences a π phase change and thus the total probability of a coincidence is calculated to be

$$P_{Coincidence} = |\frac{1}{\sqrt{2}} \cdot \frac{1}{\sqrt{2}}|^2 + |\frac{i}{\sqrt{2}} \cdot \frac{i}{\sqrt{2}}|^2 = 0 \tag{2.5}$$

The calculated coincidence probability of zero indicates that if the two photons entering the 50:50 beam splitter are completely indistinguishable in all their degrees of freedom, then both photons always exist the same output and thus resulting in no coincidences. This is the non-classical and unintuitive behaviour of photons known as quantum interference and arises from quantum mechanics requiring for one to calculate the probability amplitude of photons undergoing transmission and reflection.

2.2 Nonlinear Optics

The previous section discussed the variety of quantum systems that are currently used for quantum information science. It also mentioned that photons display many of the important characteristics needed for use in quantum information technologies. Single photons may be generated in a variety of methods, each having their own advantages and disadvantages. In this section we discuss the generation of single photons through the promising method of nonlinear optics.

2.2.1 Generation of Single Photons

The ideal single photon source for use in quantum photonics , is a source that will generate single photons on demand with the specific properties that are required by the user. The properties of the single photons will depend on the photon's degrees of freedom which may include specified spatial, temporal, energy and polarisation states. Additionally, a very desirable property of the single photon source is the ability to generate photons on demand. This is currently very hard to achieve without increasing the probability of generating two or more photons at the same time. However, the demand for the generation of single photons with the desirable states, comes with the requirement for the ability to accurately characterise these sources of single photons.

Currently there are many active areas of research into the generation of single photons. The commonly investigated area are atom-like sources such as quantum dots [18], nitrogen vacancy centers [19] and trapped atoms [20, 21] that are based on exciting the atom where then a single photon is emitted as it decays to its ground state (see Fig. 2.3). However the biggest problem with such sources are the capturing techniques of single photons that are generated. Another challenge is the generation of indistinguishable

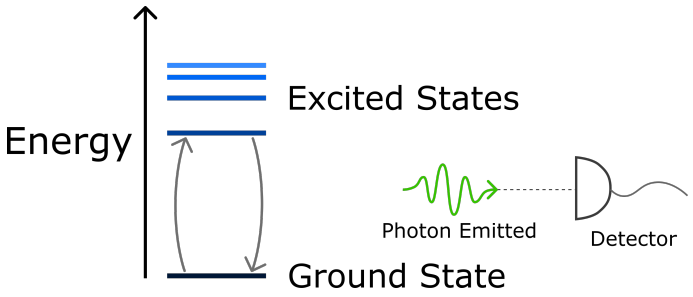

FIGURE 2.3. Atom-like source that emits a single photon when the atom decays from its excited state to it's ground state.

photons from separate sources. And of course, there is the challenging task of capturing the photons that are emitted from such sources as they can radiate in any direction.

Another way to generate single photons is the attenuation of a laser source. This consists on placing an opaque like material in front of a classical pulsed laser source, to reduce the output from the billions of photons to single photons (see Fig. 2.4). However, there are many large problems associated with such method. As this method requires very large attenuation of the classical pulses, most of the time there are no photons detected at the output. However when there are single photons at the output, more often than not depending on the attenuation level, two or more photons are detected at the same time and thus introduce noise to the detection of the photons.

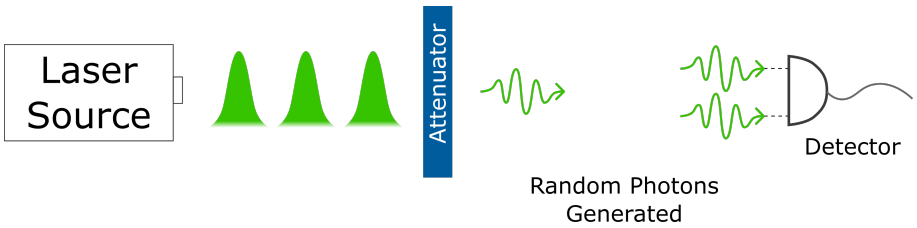

FIGURE 2.4. Schematic illustration of a single photon source by the attenuation of a laser source.

A promising method of generating single photons is using nonlinear optics. In nonlinear optics, we are able to generate heralded single photons based on the detection of a photon to determine the presence of the other photon. In this method, we use a pulsed laser to pump a nonlinear media instead of attenuating the laser like the previous method. Although in this case we are still bound by the multi-photon events in the output, what distinguishes this method from the previous method is that with each photon generated, there exists another photon that is generated simultaneously

through the nonlinear optical process (see Fig. 2.5). The generation of photon pairs in the nonlinear media allows for extraction of the time information about the creation of one photon when detecting the other. This is known as heralding and is widely used in quantum information processing [22–24]. It has been demonstrated that with the heralding information, probabilistic sources can be multiplexed to near-deterministic sources [25].

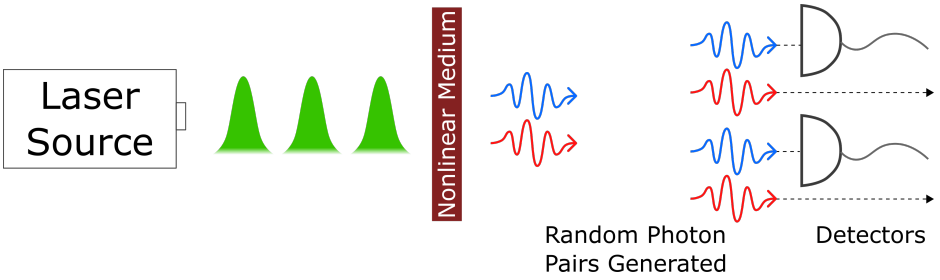

FIGURE 2.5. Schematic illustration of photon pair generation in a nonlinear medium, allowing for the heralding of the partner photon.

A mature process for the generation of single photons is a third order nonlinear process called spontaneous four-wave mixing (FWM) that takes place in χ^3 nonlinear mediums. It is important to note that although nonlinear optics offers a great advantage over the attenuation of laser, the ratio of the generation of single-pair photons to multi-pair photons are still governed by Poissonian and thermal statistics. However, since the process of pair generation in nonlinear media must satisfy the energy and phase matching conditions (explained in detail in Sec. 2.2.3), this disadvantage is negated with the ability to herald photons.

2.2.2 Photon Statistics and Coincidences

The generation of photon pairs via spontaneous FWM and spontaneous parametric down-conversion (PDC) have yet to be perfected - in practice, the detection of photon-pairs is easily degraded before detection, as the result of coupling losses into the device, propagation losses and detection efficiencies. Therefore, it is necessary to completely characterise the nonlinear device to understand the exact photon statistics of the photon-pairs generated. To do this, one can characterise the source using the coincidence to accidental ratio (CAR) [26].

Referring to Fig. 2.6, consider a scheme where a pulse laser is input into a nonlinear device, generating a continuous stream of photon pairs. Traditionally the higher energy

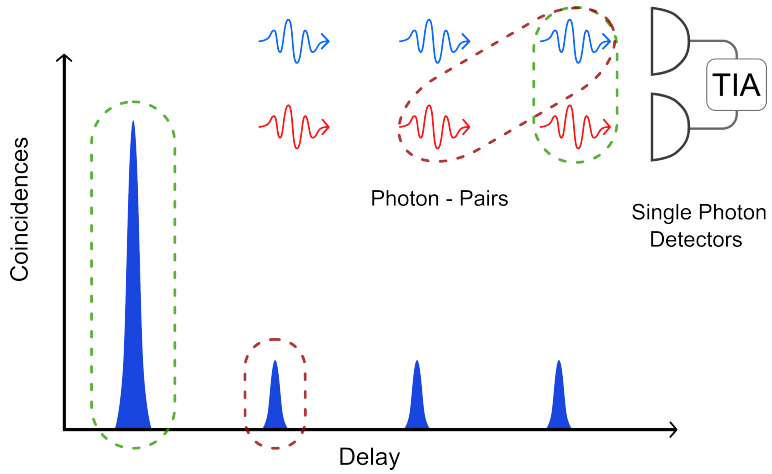

FIGURE 2.6. A typical CAR histogram is shown. Inset shows single photon pairs reaching a pair of single photon detectors. Photon-pair arrival times are analysed using a TIA which are then used in a CAR histogram.

and lower energy photons are named signal and idler photons respectively. The pair of signal and idler photons are then detected via two single photon detectors where the arrival times of each photon is analysed. This is referred to time-tagging and is made possible with the use of an electronic time interval analyser (TIA). Using the TIA, a correlated photon pair detection from the same pulse is referred to a coincidence, C, shown in the inset of Fig. 2.6 via the green dashed oval. Plotting the number of coincidences in a CAR histogram such as the one in Fig. 2.6, yields a large peak at 0 delay.

If we look at the delay between the signal and idler photons from one or more pump pulses, we will obtain smaller coincidence peaks in the CAR histogram at different delays. The delay between the smaller peak and the previous peak corresponds to the delay between the detection of the signal and idler photons (illustrated by the red dashed oval in Fig. 2.6). The smaller peaks are named accidental coincidences, A, measured as a result of multi-pair spontaneous FWM generation, leaked pump photons and single photon detection in the absence of light (dark counts). The CAR can be mathematically defined as

$$CAR = \frac{C - A}{A}. \tag{2.6}$$

In quantum photonics, the numerator term $C-A$, is often defined as the true coincidences and encompasses coincidences from actual signal and idler pairs that are generated from

the nonlinear device. The CAR is an important measurement in quantum photonics that gives insight to the photon pair generation statistics of the nonlinear device.

2.2.3 A Brief History of Nonlinear Optics

With the invention of the laser in 1960, it was discovered that the response of atoms in a high intensity electromagnetic field could no longer be considered to be linear in the electric field. This finding was named nonlinear optics and can be first traced back to 1961, with the first observation of the nonlinear optical effect, second harmonic generation [27]. By pumping a quartz crystal with a ruby laser beam (λ = 694.2 nm), Franken et al. were able to observe ultraviolet light at twice the frequency (λ = 347.1 nm). After this discovery soon followed with the breakthrough of a large number of nonlinear processes including three-wave and four-wave mixing in second and third order nonlinear media respectively [28, 29].

As the field of nonlinear optics began to grow with improved lasers and refined metrology, quantum mechanics and the theorised description of quantised light pushed to the discovery of a new field of science; quantum optics. In 1982 the first demonstration of correlations of linear polarisation of pair of photons generated via cascaded calcium atoms were demonstrated [30]. However, it was not until 1992 at the IBM Research Division that showed it is this property of quantum mechanics that is critical to the development of quantum communication and cryptography [31].

In quantum optics, the leading method for the generation of single photons is based not only on spontaneous FWM but spontaneous PDC in χ^2 nonlinear media as well. Currently, the most mature platforms for the generation of entangled photon pairs include silicon nanowire waveguides and periodically poled lithium niobate (PPLN) media for spontaneous FWM and PDC respectively. However, silicon continues to be one of the most investigated platforms due to it's potential for the generation of correlated photon pairs on the millimetre scale but efficient fabrication with the current mature fabrication technologies. Furthermore, as we are moving towards complex quantum optic technologies, the demand for the generation of photons with specific states continues to grow exponentially. As such, a big challenge is the characterisation of these photon pair sources that are generated though these nonlinear devices.

2.2.4 Four-Wave Mixing

In classical optics, light can be described as the propagation of synchronised oscillation of electric and magnetic fields which has been very successful in the explanation of the macroscopic behaviour of light, such as diffraction and interference. The mathematical description of classical light is given by the Maxwell's equations of the form

$$\nabla \cdot \vec{D} = \rho \tag{2.7}$$

$$\nabla \times \vec{H} - \frac{\partial \vec{D}}{\partial t} = \vec{J} \tag{2.8}$$

$$\nabla \times \vec{E} + \frac{\partial \vec{B}}{\partial t} = 0 \tag{2.9}$$

$$\nabla \cdot \vec{E} = 0, \tag{2.10}$$

where $\vec{J}$ and ρ are the free current and charge densities respectively. $\vec{H}$ is the magnetic field, $\vec{E}$ is the electric field and $\vec{B}$ is the magnetic induction. Finally, $\vec{D}$ is the electric displacement field is related to $\vec{E}$ through the polarisation field $\vec{P}$ in a medium given by

$$\vec{D} = \vec{E} + \vec{P}, \tag{2.11}$$

Most often in optics, the polarisation field is considered to be linearly related to the incidence electric field via the electric susceptibility χ [27], given by

$$\vec{P} = \chi \vec{E}. \tag{2.12}$$

While this consideration is true for low intensity electric fields, in reality at large enough field strength this equation no longer valid and thus requires a more complicated relation equation. Therefore, a more accurate can be obtained by expanding the polarisation in Taylor series [32]

$$\vec{P} = \chi^{(1)}\vec{E} + \chi^{(2)}\vec{E}^2 + \chi^{(3)}\vec{E}^3 + ... \tag{2.13}$$

where the first coefficient, $\chi^{(1)}$, is the linear electric susceptibility that was previously discussed and $\chi^{(2)}$ is the second order susceptibility that is responsible for second harmonic generation, three wave mixing, electro-optic effect and PDC. $\chi^{(3)}$ is the previously mentioned third order susceptibility that is responsible for third harmonic generation, the optical Kerr effect and FWM.

Because silicon platforms can be cheaply fabricated compared to other nonlinear platforms and offer the potential for integration with microelectronic chips, in the past

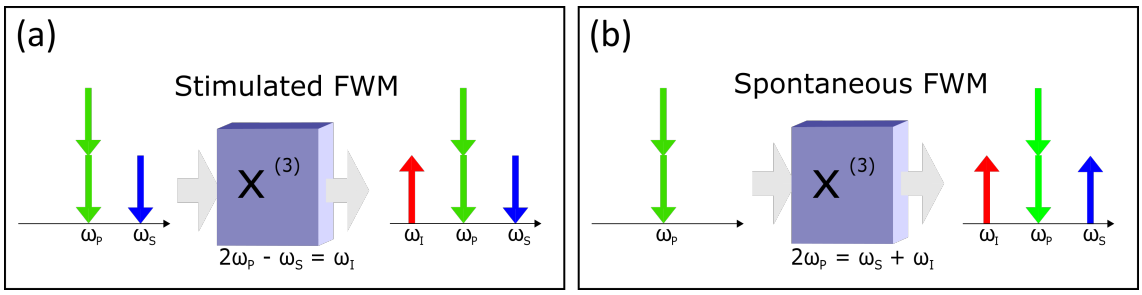

FIGURE 2.7. Illustration of (a) classically stimulated FWM process and (b) spontaneous FWM.

few years FWM has been one of the widely investigated nonlinear processes. FWM is the elastic scattering of two beam of photons into different frequencies. This nonlinear process can take place in two regimes: non-classically or classically with or without an input seed together with the pump beam respectively. Referring to Fig. 2.7, both the classical and non-classical FWM processes must obey energy conservation such that

$$0 = \omega_s + \omega_i - 2\omega_p \tag{2.14}$$

where ω_p,ω_s and ω_i are the pump, signal and idler frequencies respectively. In quantum photonics, the non-classical (quantum) process is termed spontaneous FWM as it relies on random vacuum fluctuations of the electromagnetic field to generate photon pairs [33]. The classical process is termed stimulated FWM and is the high-gain process of the two, that occurs with an additional classical input field (denoted as the seed) in either the signal or idler band. In stimulated FWM, the first pair of photons are generated spontaneously and then act as seeds for the for the sub-harmonic field due to the high amplification in the device [28]. As such, stimulated FWM is much more efficient than it's quantum counterpart; spontaneous FWM. In addition to the conservation of energy, both FWM processes must also satisfy the conservation equation

$$0 = k_s + k_i - 2k_p + 2\gamma P_p \tag{2.15}$$

where $k_j = \frac{\omega_j n_{j(\omega_j)}}{c}$ for $j = p,s,i$ represents the wave vectors of the pump, signal and idler frequencies respectively. The term, $2\gamma P_p$, consists of the nonlinear coefficient γ, and peak pump power P_p that takes into account the phase mismatch induced by other nonlinear effects such as self-phase and cross phase modulation in the device. The nonlinear coefficient γ is given by

$$\gamma = \frac{2\pi n_2}{\lambda_p A_{eff}} \tag{2.16}$$

where λ_p is the pump wavelength, A_{eff} is the effective mode area and n_2 is the nonlinear refractive index.

2.2.5 Nonlinear Devices

To achieve high FWM efficiency, a suitable $\chi^{(3)}$ nonlinear medium that fully satisfies the energy and phase-matching conditions is required. The nonlinear medium must also allow for precise control over the generated photon degrees of freedom. In recent years, there have been many nonlinear mediums that posses high FWM efficiency with control over the light. Leading examples of such devices include highly nonlinear fibres (HNLF) [34], As_2S_3 waveguides [35] and silicon nanowires waveguides [36].

However, as discussed in Section 2.1.1, complex photonic circuits have been realised by chip-scale integration. Therefore, waveguides posses the best potential candidate for the future direction of quantum information processing. Waveguides confine light to a localised spatial mode and therefore allow precise control over the light's path and phase. In the previously mentioned nonlinear devices, the HNLF although is very commonly used due to it's maturity in fabrication and thus relatively low-cost to other on-chip waveguide platforms, it is a fibre based platform that requires light to propagate a considerable amount to achieve nonlinear phase shift. Thus HNLF is not a suitable candidate for on-chip scale integration. On the other hand, As_2S_3, although a waveguide, suffers from large Raman scattering which can introduce unwanted noise and thus posses a large problem for quantum photonic applications.

However, silicon does not suffer from Raman Scattering and due to its high nonlinearity only requires millimetres to achieve nonlinear phase shift. Silicon have been around since 2006 with the first demonstration of spontaneous FWM correlated photon pair generation in a silicon nanowire [37]. Since then, silicon has attracted tremendous attention as a promising technology in electro-optic integration for quantum computing and communication. Mainly due to the combination of high intrinsic $\chi^{(3)}$ nonlinearity, the possibility for dense integration, mature fabrication methods using complementary metal-oxide semiconductor (CMOS) processing technology, low losses and low cost [38–40], silicon photonics is currently the leading platform for on-chip quantum integrated circuits. As such, there is significant motivation to use integrated χ^3 nonlinear devices

for generating quantum correlated photon pairs in the telecommunication band and to develop fast characterisation techniques [41–48].

2.3 Quantum Entanglement

Quantum entanglement is the strange non-classical phenomenon in which two or more quantum particles are linked together in a way such that the measurement of one particle's quantum state instantly determines the possible quantum states of the other particles. In general, quantum entanglement is a special correlation and superposition of quantum particles and is one of the most investigated and thus central principles of quantum mechanics and is the main research area of many scientific groups around the world. Quantum entanglement between photons has been realised to be a key resource for exceeding the technological limits imposed by classical physics and thus plays an integral part in many applications of quantum optics including optical quantum computing [6] and secure communication over long distances [8]. In this section we explore the principal of quantum entanglement that exists between photons and explore the quantification of a specific correlations that arises from spontaneous FWM.

2.3.1 Spectral Correlation

Different quantum information schemes require entangled or non-entangled photons. This entanglement is a quantum mechanical phenomena which allows correlation and superposition between two quantum states. If two quantum particles such as photons are entangled, then a measurement on both photons will reveal the quantum states to be random but correlated. This random correlation is the key to the many proposed schemes in quantum information science.

Quantum entanglement between photons can exist in many degrees of freedom including polarisation, time domain and energy (or frequency and wavelength) as presented in Equation 2.2. Going back to the basics, let us imagine two qubits that can each take the state $|0\rangle$ or $|1\rangle$. If we represent the two quibits as simple superposition states of two particles with maximum correlation, we arrive at the Bell states [49] given by

$$|\Psi^{\pm}\rangle = \frac{1}{\sqrt{2}}(|0\rangle_1 |1\rangle_2 \pm |1\rangle_1 |0\rangle_2) \tag{2.17}$$

$$|\Phi^{\pm}\rangle = \frac{1}{\sqrt{2}}(|0\rangle_1 |0\rangle_2 \pm |1\rangle_1 |1\rangle_2) \tag{2.18}$$

where the subscripts represents the quantum particles 1 and 2. These equations represent correlated states and cannot be divided into separate wavefunctions that describes each of the sate of particle 1 and 2 individually. In other words, the quantum state of particle 1 (2) is inherently linked to the state of particle 2 (1).

In the example of quantum states in Equation 2.18 for particles 1 and 2, arbitrary states of $|0\rangle$ or $|1\rangle$ were chosen. However the same equations can be written for the other photons degrees of freedom. In quantum optics, a specific example of a quantum entanglement is energy (and thus frequency) and time-bin correlations given by [50, 51]

$$|\Psi^{\pm}\rangle = \frac{1}{\sqrt{2}}(|\omega_i\rangle_1 |\omega_s\rangle_2 \pm |\omega_{i'}\rangle_1 |\omega_{s'}\rangle_2), \tag{2.19}$$

$$|\Psi^{\pm}\rangle = \frac{1}{\sqrt{2}}(|E\rangle_1 |E\rangle_2 \pm |L\rangle_1 |L\rangle_2), \tag{2.20}$$

where ω_i and ω_s are the different angular frequencies of idler and signal photons respectively, and E is the early and L is the late time-bin of photons 1 and 2. The specific correlations in Equations. 2.19 and 2.20 are known as spectral correlation that arises naturally in spontaneous FWM and is the focus of this thesis. As mentioned previously in section 2.1.2, to perform quantum interference, we require both photons to contain the exact same degrees of freedom including energy (or conversely frequency) and time-bin modes. Therefore it is important to understand that photons that are generated in states that are presented in Equations 2.19 and 2.20 will eliminate the indistinguishability of photons and therefore does not allow for quantum interference. The focus of this thesis is the accurate and precise measurement of this spectral correlations of photon pairs that are generated through spontaneous FWM.

2.3.2 Joint Spectral Intensity and the Schmidt Number

The experimental characterisation of spectral correlations between photons has a been an on-going task in quantum photonics, where there have been several proven methods of measuring the spectral correlations of photons. The most popular methods of characterisations are summarised in the Table. 2.2 below.

However, a established method of characterising the spectral correlations between photons consists of measuring the joint spectral intensity (JSI). This is a mature technique that has been used frequently in quantum optics and photonics to determine the joint spectral state of the signal and idler photons that are generated via spontaneous FWM

Method	Description
Hung Ou Mandel	Indistinguishable photons will result in a drop in coincidences when the photon's temporal degree of freedom overlap [52].
Quantum Homodyne Tomography	Reconstruction of the complete quantum state of photon pairs through a series of measurements in different basis to obtain the density matrix [53].
Joint Spectral Intensity	A coincidence based measurement of where the degree of spectral correlations between photon pairs will give different joint spectral intensity plots [54].

Table 2.2: A summary of current methods used to characterise the spectral correlations of photon-pairs generated via spontaneous FWM and spontaneous PDC.

and spontaneous PDC [24, 55, 56]. Through the JSI, one is able to quantify the degree of spectral entanglement by performing what is referred to a Schmidt decomposition.

For a guided-mode co-polarised photon generation via spontaneous FWM, the two-photon output output squeezed state can be simply expressed as

$$|\Psi_{s,i}\rangle = \iint A(\omega_i,\omega_s)\,|\omega_i\rangle\,|\omega_s\rangle\,d(\omega_i)d(\omega_s), \tag{2.21}$$

where $|\omega\rangle = \hat{a}^{\dagger}_{\omega}|\text{vac}\rangle$ is the state containing a single photon in the waveguide mode at ω, represented by the creation operator acting on the vacuum state. The $A(\omega_i,\omega_s)$ term is known as the joint spectral amplitude (JSA), defined as

$$A(\omega_i,\omega_s) = \int \alpha(\omega)\alpha(\omega_i+\omega_s-\omega)\phi(\omega_i,\omega_s,\omega), \tag{2.22}$$

where the function $\alpha(\omega)$ is the complex amplitude of the pump spectrum with centre frequency ω_p and $\phi(\omega_i,\omega_s,\omega)$ is the phase-matching function of the waveguide that encompasses the waveguide material design and optical properties. The JSA is expanded more in detail in the next chapter. It should be noted that the square modulus of the JSA, $|A(\omega_i,\omega s)|^2$, is defined as the JSI where experiments to date have been measuring. Fig. 2.8(a) illustrates a typical JSI measurement that is a function of the pump and phase-matching profile of the nonlinear device.

As the JSA is a complex function of two variables, to fully analyse the function, the JSA must be written in a factorable state. A factorable state is defined as a state from which the JSA is a product of two functions

$$A(\omega_i,\omega_s) = I(\omega_i)S(\omega_s), \tag{2.23}$$

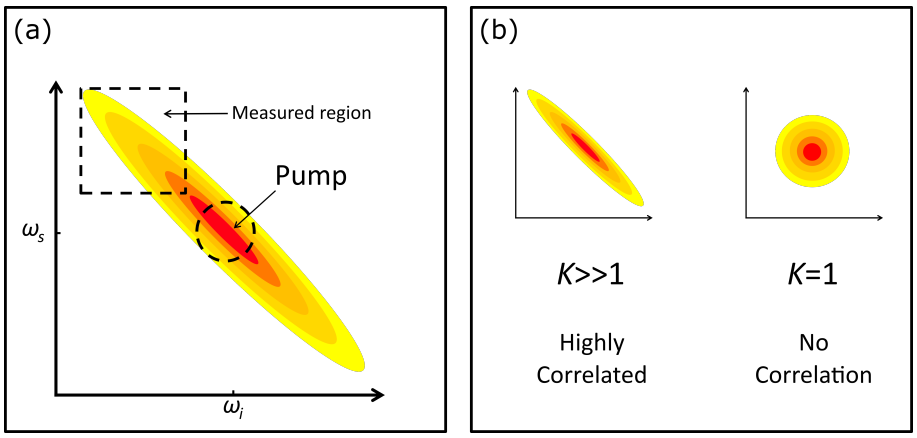

FIGURE 2.8. A typical (a) JSI measurement with the centre pump frequency highlighted and (b) JSI measurement for no correlation ($K = 1$) and high correlations ($K >> 1$) between the signal and idler photon pairs.

where the functions $I(\omega_i)$ and $S(\omega_s)$ are dependent only on the idler and signal frequencies respectively. Now that the JSA is expressed as two variables, the JSA can be fully characterised by the Schmidt decomposition, by which it is expressed as a linear combination of the form

$$A(\omega_i, \omega_s) = \sum \sqrt{\lambda_n} f_n(\omega_i) g_n(\omega_s), \tag{2.24}$$

where $f_n(\omega_i)$ and $g_n(\omega_s)$ are each a complete set of complete factorable and orthogonal functions for idler and signal frequencies respectively [57] and λ_n are the positive real numbers that are known as the Schmidt magnitudes that must satisfy $\sum_n \lambda_n = 1$. From this Schmidt magnitudes, one can quantify the degree of spectral correlation of the photon pairs via the Schmidt number K, defined as

$$K = \sum_n \frac{1}{|\lambda_n^2|}, \tag{2.25}$$

For a completely spectrally uncorrelated photons in the system, the Schmidt magnitude is 1 for $\lambda_{n=1} = 1$, and zero for higher order n terms: $\lambda_{n\neq 1} = 0$ so that $K = 1$. However, for a completely correlated system, the higher order Schmidt magnitudes are nonzero so that $K > 1$ (see Fig. 2.8 (b)).

As mentioned earlier, obtaining the full phase dependent JSA for a photon source is experimentally challenging and thus to date has been virtually inaccessible [58]. Therefore experiments have focused on measuring the JSI for spontaneous FWM and PDC nonlinear devices. As the Schmidt decomposition given by Equation 2.24 is not

directly applicable to the JSI, the Schmidt number K is not strictly available from experiment. One method to solve this is to apply the Schmidt decomposition to the square root of the measured JSI. However it is easily seen that a measurement of the JSI results in a loss of phase information when estimating $A(\omega_i,\omega s) = \sqrt{|A(\omega_i,\omega s)|^2}$. As such when performing Schmidt decomposition to the square root of the JSI, a lower bound to the Schmidt number must be given [59]. In this thesis, I will refer to the Schmidt number lower bound (SNLB) with the symbol $\tilde{K}$.

For a specific set of two-photon states, the Schmidt decomposition is an analytical method. However, an analytical method cannot be used to determine the degree of spectral correlation for the experimentally measured JSIs. Hence, another method is required to determine the degree of spectral entanglement from the experimentally measured JSIs. Fortunately, there exists a matrix operation known as singular value decomposition (SVD), which is the matrix analogue of the Schmidt decomposition that can be computed numerically to determine the degree of spectral correlation. Let the JSA be written as

$$M = A \cdot \Phi \tag{2.26}$$

where A is the matrix corresponding to the pump envelope and Φ is the matrix corresponding to the phase matching function. By performing SVD, M is factorised into three separate matrices to be called I,D,S. The columns of I and S represent the Schmidt states related to the idler and signal frequencies respectively with D being the diagonal matrix containing the Schmidt magnitudes that links two matrices such that

$$M = I \cdot D \cdot S^* \tag{2.27}$$

$$M = \begin{pmatrix} I_{1,1} & I_{1,2} & \cdots & I_{1,k} \\ I_{2,1} & I_{2,2} & \cdots & I_{2,k} \\ \vdots & \vdots & \ddots & \vdots \\ I_{j,1} & I_{j,2} & \cdots & I_{j,k} \end{pmatrix} \cdot \begin{pmatrix} \sqrt{\lambda_1} & 0 & \cdots & 0 \\ 0 & \sqrt{\lambda_2} & \cdots & 0 \\ \vdots & \vdots & \ddots & \vdots \\ 0 & 0 & \cdots & \sqrt{\lambda_n} \end{pmatrix} \cdot \begin{pmatrix} S_{1,1} & S_{2,1} & \cdots & S_{j,1} \\ S_{1,2} & S_{2,2} & \cdots & S_{j,2} \\ \vdots & \vdots & \ddots & \vdots \\ S_{1,k} & S_{2,k} & \cdots & S_{j,k} \end{pmatrix} \tag{2.28}$$

where S^* is the conjugate transpose of matrix S [60]. From this, one can use Equation 2.25 to calculate the Schmidt number. In the next chapter, we apply SVD to numerical simulation of the JSI and compare that to experimental measurements.

CHAPTER 3

JOINT SPECTRAL INTENSITY

In the previous chapter, we examined the demand for spectral correlation of photon pairs in the field of quantum optics and investigated the importance of characterisation of photon pair sources generated through the JSI measurement. In summary, this chapter consists of

- An in depth look at the theoretically-calculated model of the JSI.
- Detailed investigation of current methods used to measure the JSI in the quantum regime that is based on temporal and spatial mode separation of photon pairs.
- Introduction to JSI measurement in the classical regime using stimulated processes.
- Comparison of JSI measurements between the quantum and classical processes in an integrated $\chi^{(3)}$ nonlinear device.

This chapter is based on the following publication:
I. Jizan, L.G. Helt, C. Xiong, M.J. Collins, D.Y. Choi, C.J. Chae, M. Liscidini, M.J. Steel, B.J. Eggleton and A.S. Clark, "Bi-photon spectral correlation measurements from a silicon nanowire in the quantum and classical regimes.", *Scientific reports*, **5**, 12557, (2015).

3.1 Theoretical Model

To theoretically model the JSI, we will need to consider and investigate each component of equation 2.22 individually. In the following section, we will theoretically calculate and plot the pump and phase matching function for a standard $\chi^{(3)}$ device which then are used to plot the final JSI.

3.1.1 Pump Envelope Function

Generally, the input pump for the generation of signal and idler photon pair often has a temporal shape that can be approximated with a Gaussian function. Additionally, as all of our pumps that are used to obtain JSI measurements have a Gaussian profile, we can therefore approximate the pump envelope function as

$$a(\omega) \approx \frac{1}{\sigma\sqrt{2\pi}} e^{-\frac{\omega^2}{2\sigma^2}} \tag{3.1}$$

where σ is the standard deviation of the Gaussian pump pulse in angular frequency, given by

$$\sigma = \frac{2\sqrt{ln(2)}}{T} \tag{3.2}$$

where T is the pump pulse temporal width at full-width at half maximum (FWHM), typically in the orders of picoseconds. It is evident from the JSA equation 2.22 in Chapter 2, that the pump function term accepts the sum frequencies of signal and idler photons, to give a symmetric distribution between the signal and idler frequencies.
By evaluating equation 3.1 for signal and idler frequencies, and for a standard 10 ps pump pulse temporal width, the pump function is plotted in Fig. 3.1. As expected, a cross-sectional horizontal or vertical view across Fig. 3.1 will have a Gaussian profile. One thing to note from equations 3.1 and 3.2 is that an increase in pump pulse temporal width will result in a decrease in the thickness of the anti-diagonal (-45°) band in Fig. 3.1.

3.1.2 Phase-Matching Profile

For the separate generation of signal and idler photons, we must consider the nonlinear properties of the nonlinear devices accordingly. As the phase-matching of the nonlinear device must satisfy certain boundary conditions [61], the natural phase-matching function in equation 2.22 is described by

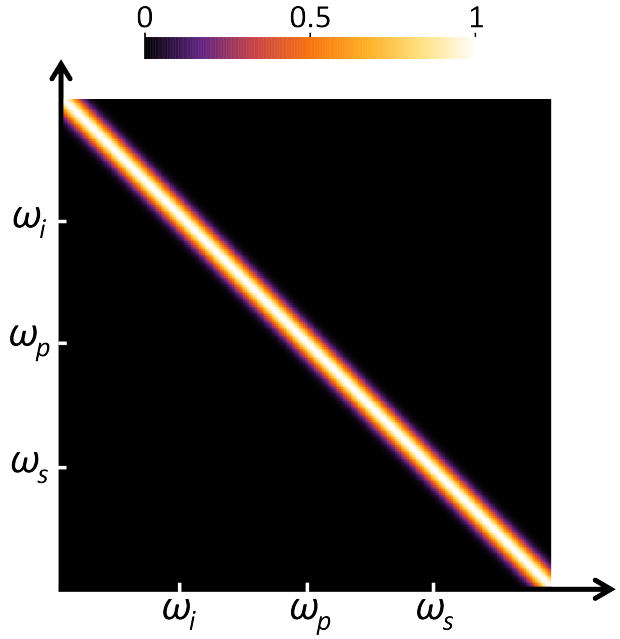

FIGURE 3.1. Normalised theoretically calculated model of the pump function, for a typical pump pulse width of 10 ps.

$$\phi(\omega_s,\omega_i) = \frac{1}{\sqrt{2\pi}} sinc\left(\frac{\Delta kL}{2}\right) e^{i\Delta kL/2} \tag{3.3}$$

where L is the length of propagation of light in the device and Δk is the phase-mismatch function around the phase-matched frequencies given by

$$\Delta k = k_s + k_i - 2k_p + 2\gamma P_p. \tag{3.4}$$

This phase-mismatch represents the detuning from the perfect and efficient phase-matching given by equation 2.15. As Δk can be expressed as

$$k(\Omega) = \frac{\omega n(\omega)}{c_0} \tag{3.5}$$

where $n(\omega)$ is the frequency dependent refractive index of the nonlinear device and c_0 is the speed of light in vacuum, we can estimate the phase-mismatch, by the Taylor expansion about the centre frequency, ω

$$k(\Omega) = k_0 + \frac{dk(\omega)}{d\omega}(\omega_p - \omega) + \frac{d^2k(\omega)}{d\omega^2}\frac{1}{2}(\omega_p - \omega)^2 + ... \tag{3.6}$$

where k_0 is the phase velocity. In nonlinear optics, the inverse of the first derivative of the wavevector with respect to angular frequency is defined as

$$\frac{dk(\omega)}{d\omega} = \frac{1}{v_g}, \tag{3.7}$$

where v_g is the group velocity of the light in the medium. The second derivative of the wavevector with respect to angular frequency is defined as

$$\frac{d^2k(\omega)}{d\omega^2} = \frac{d}{d\omega}\left(\frac{1}{v_g}\right) = GVD, \tag{3.8}$$

where GVD is the group velocity dispersion. GVD describes the phenomenon in which the group velocity, v_g, of light in a medium depends on it's optical frequencies or wavelengths. In optical waveguides, the GVD is usually defined as the derivative with respect to wavelength, λ, expressed as

$$D_\lambda = -\frac{2\pi c}{\lambda^2} \cdot GVD, \tag{3.9}$$

where D_λ is the simply the dispersion of the nonlinear waveguide, usually specified with units of picoseconds per nanometre-kilometre (ps/(nm-km)). From the previous chapter, we saw that for FWM to take place, the energy matching condition must be satisfied such that the sum of the energies of the idler and signal photon must equal to two pump frequencies. Therefore, the phase-matching function can be thought as a function that determines how the energy of the pump is to be distributed.
For the simulation of the JSI, we therefore require the the group velocity and GVD (or dispersion) for use in equation 3.3 to calculate and model the phase matching function. In Fig. 3.2, we have plotted the phase matching function for a typical waveguide with a $k_0 = 9.63 \times 10^6$ $v_p = 7.02 \times 10^7$ m/s and $GVD = -6.03 \times 10^{-25}$ s^2/m.

3.1.3 Joint Spectral Intensity

Now that we have successfully modelled the pump and phase matching function, we can now theoretically calculate and simulate the JSI by solving and then squaring equation 2.22.
In Fig. 3.3, we have plotted the JSI for the pump profile and phase-matching parameters that were used in the separate plots of the pump and phase-matching functions in the previous sections. It is often useful to think of the JSI plotted in Fig. 3.3 as a multiplication of Fig. 3.1 and Fig. 3.2. Again, it is important to note that the JSI plot in Fig. 3.3 is the square of the JSA that is define in equation 2.22. As mentioned in section 3.1.1, an increase in the temporal width of the pump will result in a narrower

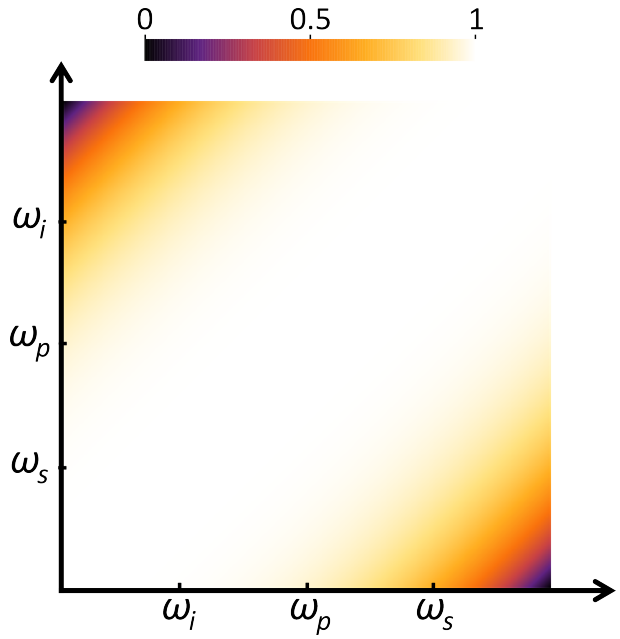

FIGURE 3.2. The normalised theoretically calculated model of the phase matching function for a waveguide with a $k_0 = 9.63 \times 10^6$ $v_p = 7.02 \times 10^7$ m/s and $GVD = -6.03 \times 10^{-25}$ s^2/m.

anti-diagonal, -45° band in Fig. 3.1. As you would predict, this will also result in the final JSI to contain a narrower anti-diagonal band. In other words, this leads to an increase in correlations between the signal and idler photons and therefore an increase in the SNLB, $\tilde{K}$, as we will see in the next sections.

3.2 Previous Quantum Measurement Schemes

As mentioned in the previous chapter, a JSI measurement is a well established method of characterising the spectral correlations of photon pairs that are generated via $\chi^{(2)}$ and $\chi^{(3)}$ nonlinear devices. Traditionally, this consist of coincidence based measurement where the correlated photon pairs generated via spontaneous FWM and spontaneous PDC are directed to photon detectors where they are analysed for coincidences. In general there exists two experimental approaches for the detection and analysis of coincidences between the correlated photons pairs as illustrated in Fig. 3.4 and Fig. 3.5.

The most popular method of coincidence based JSI measurement is commonly termed the temporal dispersion method that relies on dispersion to temporally stretch the single photon pulses and spectrally resolve them in the time domain [55, 59, 62].

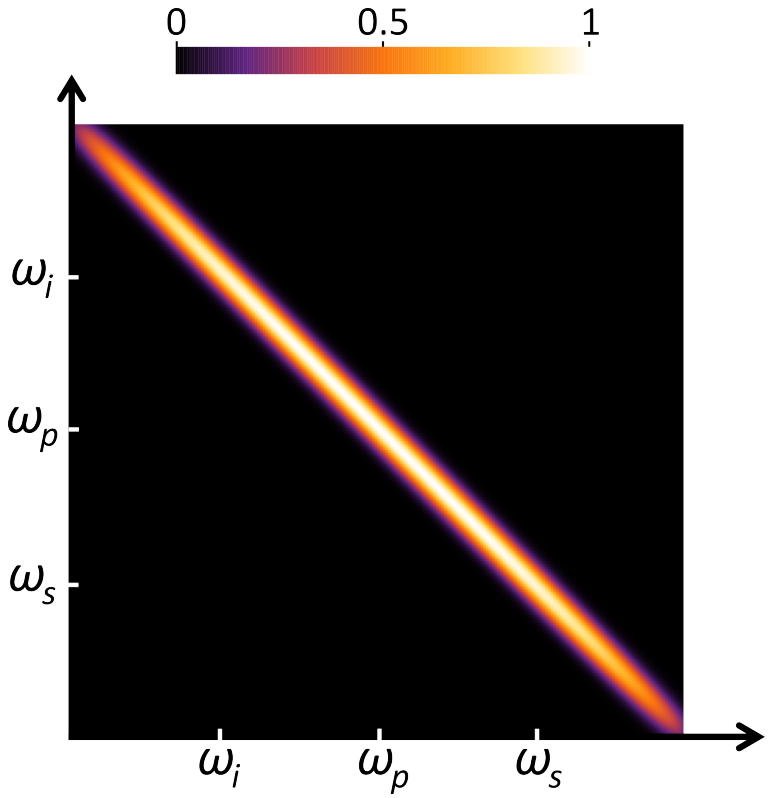

FIGURE 3.3. The final normalised theoretically calculated model of the JSI for a pump and phase matching functions given in the previous sub-sections.

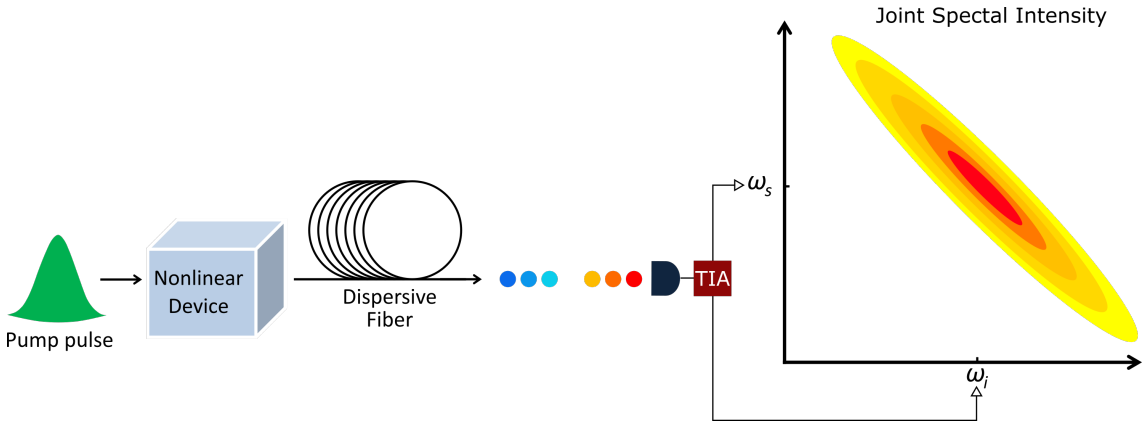

FIGURE 3.4. The conventional approach for a JSI measurement consisting of a highly dispersive fibre that temporally separates the signal and idler photons. The stream of signal and idler photons are detected and time tagged using a TIA to build a JSI plot.

As shown in Fig. 3.4, when the correlated photon pairs are generated via the nonlinear device, the generated signal and idler photons are directed into a dispersive fibre with a specific dispersion. Because photons of different wavelengths have different group velocities in the dispersive fibre, the propagation times of each individual photons through the dispersive fibre are different. As a result, by using a single photon detector and a TIA, each individual photon is time-tagged by measuring the transit time in the dispersive fibre which therefore yields a measure of the photon wavelength. With each time tag of all the single photons that are detected, post processing allows for the analysis and calculation of coincidences at each pair of frequency where one is able to then build a JSI plot. The drawback with this method is resolution of the TIA which that in turn affects the resolution of the JSI plot. Additionally, the timing jitter of the TIA and the jitter of the single photon detectors can have a considerable impact when time tagging the photons and therefore can again limit the obtainable resolution of the JSI. In principle however, we are able to increase the resolution of the measurement of the JSI by increasing the fibre length, at the cost of higher photon losses.

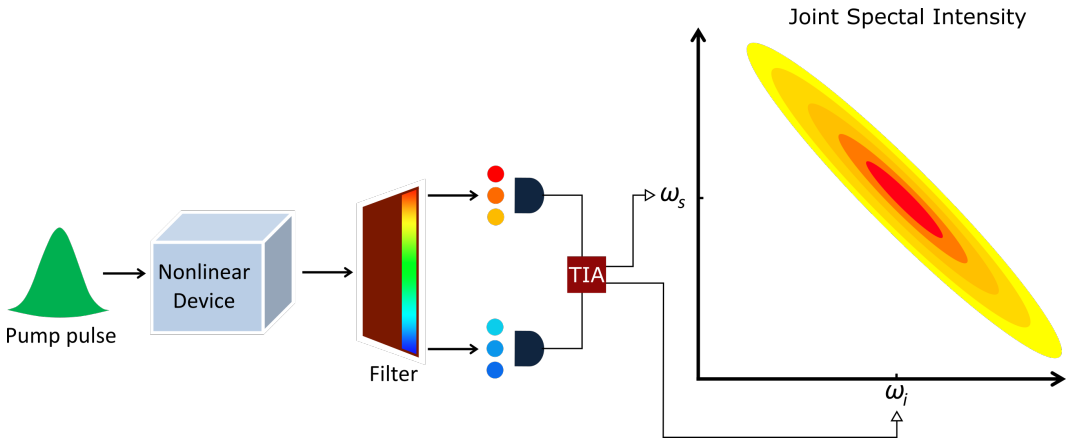

FIGURE 3.5. Another approach for a JSI measurement that uses tunable optical band pass filter to spatially separate the signal and idler photons that are generated via the nonlinear device. To measure the JSI, the wavelength of the tunable band pass filter needs to scan the FWM bandwidth of the nonlinear device.

Another approach to coincidence based measurement of the JSI is very straight forward method that requires the spatial separation of the individual signal and idler photon [24, 56]. Referring to Fig. 3.5, unlike the temporal dispersion method that temporally delays the signal and idler photons depending on their frequency, this method uses a simple tunable optical band-pass filter to separate each photon into different

spatial modes which are then detected by a pair of single photon detectors. Using the true coincidences from the CAR measurement as described in section 2.2.2, one is then able to obtain the number of coincidences between each pair of frequencies and hence build a JSI plot.

With this approach however, the resolution of the JSI is limited by the tunable optical band-pass filter. This approach requires the tunable band pass filter to separately scan the signal and idler bands (the FWM bandwidth of the nonlinear device) and measure for coincidences at each frequency pair. This can be a experimentally challenging task to accomplish depending on the stability of the of the nonlinear device. A solution to this is to automate this process by using a programmable optical band pass filter, to raster scan the signal and idler frequencies as demonstrated in [54]. Compared to the temporal dispersion method where coincidences appear randomly across the JSI, this method can target individual elements of the JSI. However, a disadvantage of this method is that when measuring a single element of the JSI, photons at the different frequencies are dropped. Therefore for a full measurement of the JSI, the acquisition time required to acquire a reasonable amount of coincidences for a pair of frequency can be very large depending on the efficiency of pair generation of the nonlinear device. Below in Fig. 3.6, are two JSI measurements of two different nonlinear devices that uses the temporal dispersion method [55] and spatial separation method [54] to measure for coincidences of photon pairs generated via spontaneous PDC and FWM respectively.

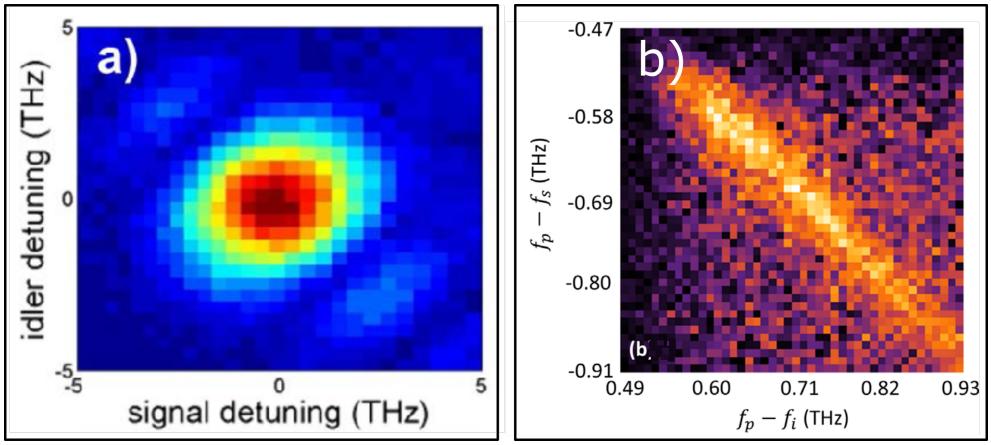

FIGURE 3.6. Two coincidence measured JSIs of photon pairs in the telecommunication band using (a) temporal dispersion method for spontaneous PDC process with resolution of 1.2 nm and (b) spatial separation method for spontaneous FWM process with a resolution of 80 pm.

3.3 An Alternative to Quantum Measurements

To address the limitations faced with quantum measurements of the JSI which requires measurement of coincidences between photon pairs, Liscidini and Sipe introduced a technique known as stimulated emission tomography (SET) to reconstruct the JSI by using the classical analogue of spontaneous photon pair generation; stimulated nonlinear wave mixing [63]. In the case of FWM discussed in section 2.2.4, stimulated FWM requires a classical seed field in either the signal or idler band, instead of relying on vacuum fluctuations to seed the conversion of a pair of pump photons into correlated signal and idler photons. This approach uses the understanding and observation that for a given pumping scheme and nonlinear device, the spontaneous and stimulated frequency conversion response functions can be made mathematically identical.

This was first demonstrated in $\chi^{(2)}$ device, namely a AlGaAs ridge waveguide, where the spontaneous process of PDC was compared to the stimulated process of difference frequency generation (DFG) [59]. This experiment compared the JSIs obtained from spontaneous PDC via the temporal dispersion method and stimulated DFG via an optical spectrum analyser (OSA). The stimulated process using DFG produced a higher resolution in only a third of the collection time with no use of single photon detectors. There have also been two demonstrations of the reconstruction of the JSI via stimulated FWM in a $\chi^{(3)}$ nonlinear birefringent optical fibre and a silicon ring-resonator based photonic chip [64, 65]. The first work compared the JSI obtained from the stimulated process to that taken by the coincidence measurements on a similar, though not identical fibre and finding close resemblance. The second work compared the JSI obtained from the stimulated process to a theoretical model finding good agreement between the two.

In this experiment we applied the stimulated process concept to an integrated $\chi^{(3)}$ nonlinear device, in this case a silicon nanowire (SiNW), and compare the results to quantum measurements for two different pump pulse widths. In the next sub-sections, we measure three JSIs, one via coincidence measurements from spontaneous FWM, and two via stimulated FWM using different detection methods. The classical stimulated FWM produces fast and reliable results, which can be readily extended to larger frequency ranges and are directly applicable to many future integrated nonlinear devices. Moreover, as the JSI is a function of the pump and phase matching profiles, we observe and compare the change in the spectral correlation of photon pairs generated using two different pump pulses durations in the nonlinear device.

We demonstrate three distinct methods of obtaining JSIs from a $\chi^{(3)}$ SiNW using,

quantum, singles-based and OSA measurements that provide progressive improvements to the signal-to-noise ratio (SNR) and measurement efficiency. Firstly, the properties of the SiNW waveguide is described in detail, describe the experimental setup used for each of the JSI measurements and then present and discuss the results obtained from these measurement setups. Furthermore, I will compare our experimental methods for two different pump pulses and compare the results to the theoretically calculated JSI models.

3.3.1 The Nonlinear Device

As sketched in Fig. 3.7(a), our nonlinear device is a 3 mm long silicon-on-insulator (SOI), 220 nm high by 460 nm wide buried SiNW, that provides an effective nonlinearity of approximately $\gamma \approx 236\ \mathrm{W}^{-1}\mathrm{m}^{-1}$.

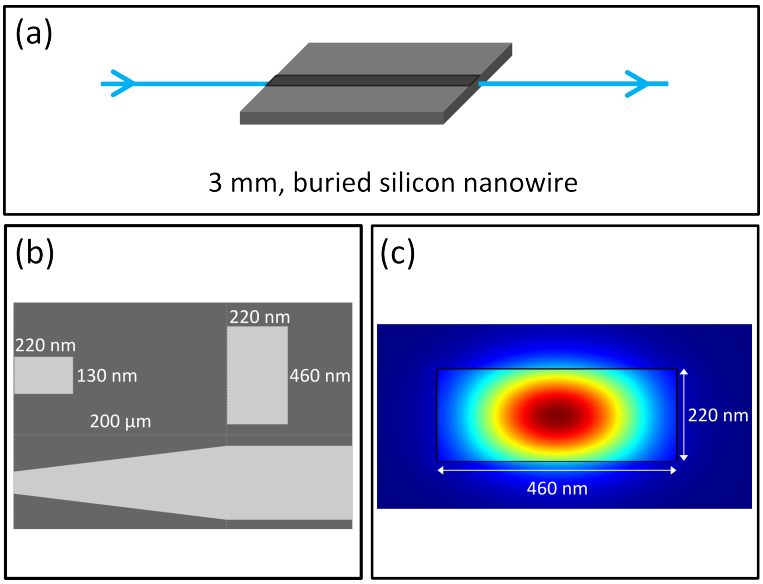

FIGURE 3.7. Schematics of (a) 3 mm Buried silicon nanowire (SiNW), the cross-sectional dimensions and (c) the simulated $|\mathbf{B}|^2$ energy density of the fundamental TE mode.

This γ was theoretically calculated via computer simulation of waveguide modes, and was used to estimate the largest average number of spontaneous FWM pairs generated on-chip per pulse within the filtering window that we could expect to observe. To ensure that we were always probing the two-photon component of our output state, the average number of spontaneous FWM pairs was kept to less than 0.1 in all measurements. Theoretically, the average number of spontaneous FWM pairs was calculated via

$$\langle N_{\text{pairs}} \rangle = \tau \Delta v (\gamma P L)^2 \, \text{sinc}^2(\frac{\Delta k L}{2}), \tag{3.10}$$

where τ is the pump temporal pulse width, Δv is the filtering of the photon pairs and L is the length of the light propagation in the nonlinear device. For our brightest measurement, using the τ = 10 ps with repetition rate of R_{rep} = 50 MHz laser at a detuning of Ω = 0.8 THz from the pump, for a Δv = 10 GHz filtering, $\langle N_{\text{pairs}} \rangle$ = 0.083 per pulse. Here the peak power $P = \frac{P_{\text{avg}}}{R_{\text{rep}} \tau}$ = 1.58 W, nonlinear device length L = 0.003 m and phase mismatch Δk = 729.0 m^{-1}. This value is corroborated by a measured pair collection rate of $R_{\text{pairs}}^{\text{measured}}$ = 1.59 per second when accounting for approximately α = 31.9 dB of losses per channel including propagation and coupling losses. Comparing this value with the theoretical pair collection rate, $R_{\text{pairs}}^{\text{theory}}$, given by

$$R_{\text{pairs}}^{\text{theory}} = \langle N_{\text{pairs}} \rangle R_{\text{rep}} (10^{-\alpha/10})^2 = 1.72, \tag{3.11}$$

we observe good agreement between theory and experiment. Note that this high peak power does have a modest effect on the phase matching condition Δk (see equation 3.4), but that any quantum time-ordering effects are expected to be quite small as we are not operating in a nearly frequency uncorrelated regime [66].

To improve waveguide to fibre coupling efficiency, the TE-optimised waveguide was inverse tapered over a 200 μ m length to a cross section of 220 nm high by 130 nm wide at the facet (see Fig. 3.7(b)). The SiNW was fabricated from a SOI wafer using standard photolithography and reactive ion etching, followed by the addition of a 2 μ m silicon dioxide upper-cladding layer deposited via plasma-enhanced chemical vapour deposition. The average power in front of the waveguide was 4.9 mW and 790 μW for the 270 ps (100 MHz) and 10 ps (50 MHz) lasers respectively. These powers were set to generate the same number of photon pairs per second in the device for the two laser pulse widths and were below the limit for two-photon absorption [67]. The average seed power in front of the waveguide was kept constant at 36.5 μW. The TE propagation and coupling losses of the SiNW were approximately 2-2.5 dB/cm and 2-2.5 dB/facet respectively. The total loss between the input and output of the SiNW was approximately 4.5 dB for all measurements.

3.3.2 Quantum Measurements

To perform quantum measurements, we employ the high resolution spatial separation method as performed in [54], to determine the JSI in the quantum regime by measuring

the correlated photon pair coincidences from spontaneous FWM. The first pump source was a pulsed fibre laser (Pritel) centred at 1550 nm (Fig. 3.8(a)) which produced 10 ps pulses with a repetition rate of 50 MHz and a 70.8 GHz spectral FWHM. The pulses are passed through a polarisation controller (PC) to select TE polarisation with respect to the SiNW waveguide. An isolator (ISO) was used to protect the laser in addition to a variable attenuator (ATT) to tune the input pump power. A narrowband tunable band-pass filter (TBPF) was used to remove any residual cavity photons from the laser. To monitor the input power entering the nonlinear SiNW, a 99:1 % fibre beam splitter with 1 % entering a power meter (PM) was used just before the SiNW.

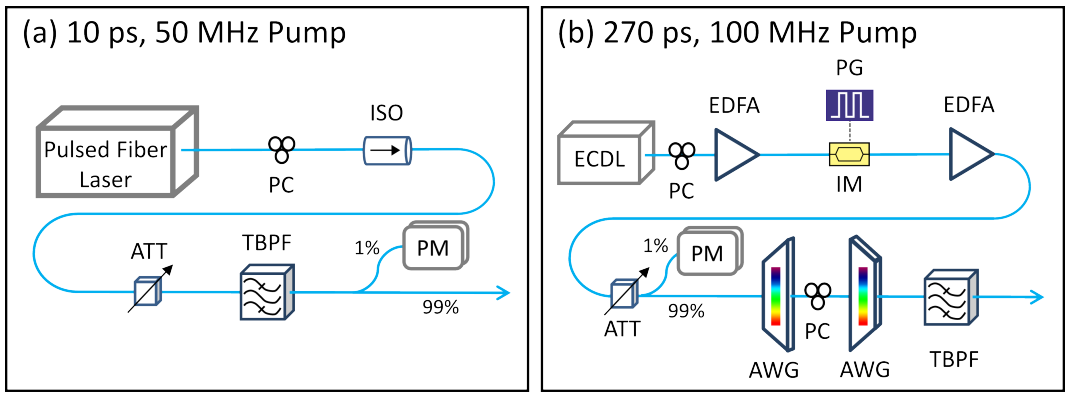

FIGURE 3.8. The experimental setup for (a) 10 ps, 50 MHz pump and (b)270 ps, 100 MHz pump. See text for a detailed description of the experimental setup.

The second pump source, shown in Fig 3.8(b), used an external diode laser (ECDL) to produce pulses with large temporal widths. The first channel of the ECDL centred at 1550 nm was passed through a PC before being pre-amplified by a low noise erbium doped fiber amplifier (EDFA). The pump was then modulated to 270 ps Gaussian pulses at a repetition rate of 100 MHz by a lithium niobate intensity modulator (IM, Sumitomo). The IM was driven by a pulse generator (PG, AVTech) resulting in a 10.4 GHz spectral FWHM. The pump pulse stream was then amplified by a second EDFA and then subsequently filtered by two arrayed waveguide gratings (AWGs, JDSU) to remove any amplified spontaneous emission noise that is produced by the EDFA. A PC was placed in between the two AWGs to adjust the polarisation such that the pump pulse was TE polarised in the nonlinear SiNW.

In the detection and analysis of the photon pairs generated by spontaneous FWM from the two different pumps, the high resolution spatial mode separation method was

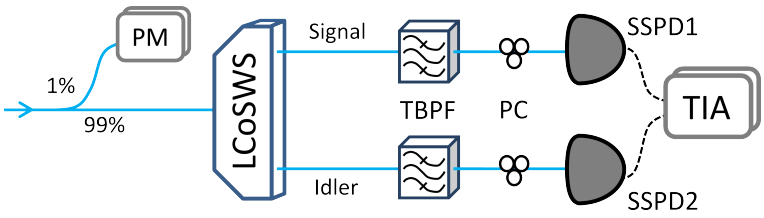

FIGURE 3.9. Schematics of the experimental setup for coincidence measurement of the JSI using the spatial separation method. See text for details.

used to measure the quantum correlations by coincidence detection. The schematics of the experimental setup for this method is shown in Fig. 3.9. A 99:1% fibre beam splitter was used to monitor the 1% output power exiting the SiNW via a PM. The remaining 99% was sent to a multi-output liquid-crystal-on-silicon waveshaper (LCoWSW, Finisar Waveshaper) that separates the signal and idler photons into two distinct spatial mode channels. The two channels were then broadband filtered to remove any residual pump photons that may have leaked into the channels. The signal and idler photons then enter two PCs before being inserted into two superconducting single photon detectors (SSPD, Single Quantum) to optimise the detection efficiency of the two channels. Coincidence measurements were conducted and recorded by a computer via a TIA (SensL). The JSI spectral resolution obtained was 10 GHz (or 80 pm), limited by the pixel bandwidth of the LCoSWS. This led to a 40×40 pixel grid for the final JSI.

3.3.3 Stimulated Measurements

For the stimulated measurements of the JSI, we emplyed an additional narrow band seed laser tuned across the signal band to stimulate classical FWM. We then measure the spectrum of the generated idler field using a single photon detector. I will refer to this method as the singles-based approach. For our second stimulated measurement of the JSI again involves the measurement of the idler field generated via stimulated FWM, but in this case using a high resolution optical spectrum analyser (OSA). I will refer to this as the OSA method.

The experimental setup for the stimulated measurement is shown in Fig. 3.10. The seed laser for the stimulated FWM experiment used the second channel of the ECDL which was also set to TE polarisation using a PC. This channel of the ECDL was computer controlled to repeatedly scan the higher-band channel of the FWM bandwidth of the SiNW over a desired range from the pump. The seed laser was combined with the 10 ps or 270 ps laser source using a 50:50% combiner and then injected injected into the SiNW

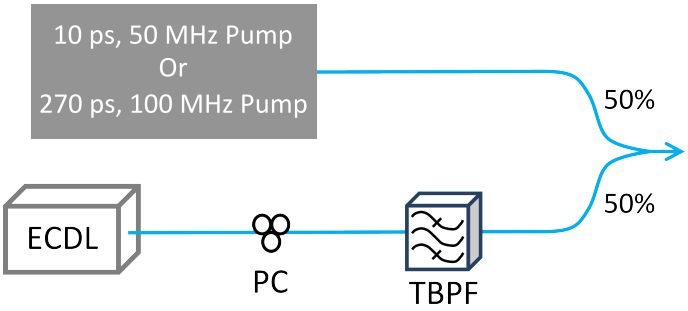

FIGURE 3.10. The seed laser used the second channel of an ECDL, set to TE polarisation using a PC and filtered clean using TBPF before being combined with the 10 ps or 270 ps laser source to stimulate FWM.

at a higher frequency than the pump, corresponding to the measured signal band in the spontaneous FWM measurements. The generated average power in the idler band was approximately 1.8 μW. Instead of performing coincidences described in Fig. 3.9, the generated idler photons was measured using the singles-based method or OSA method.

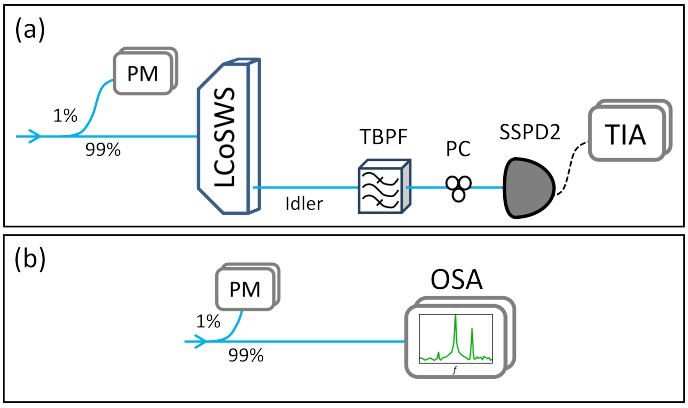

FIGURE 3.11. The experimental setup for measurement of the idler photons generated via stimulated FWM using (a) the spatial separation method and (b) an OSA. See text for details.

In the singles-based method, the generated single count rate of the idler detection band were recorded by one SSPD (as shown in Fig. 3.11(a)). Both the seed laser frequency of the ECDL and the idler detection band that is controlled by the LCoSWS were scanned in 10 GHz units in a raster scanning fashion. Again, the spectral resolution of the JSI obtained was 10 GHz with the extracted JSI represented on a 40 × 40 pixel grid. As stimulated FWM is much more efficient than its quantum counter part; spontaneous FWM, a 20 dB attenuation was applied to the LCoSWS to limit the rate of the idler

photons being detected by the SSPD and thus avoiding saturation.

The second measurement of the JSI via stimulated FWM, shown in Fig. 3.11(b), is the OSA method of measurement. In this measurement, the scanning seed laser was left untouched as in the singles-based measurement, but replaced the LCoSWS, PC, SSPD and TIA with an OSA (Yenista) that provided a higher resolution of 2.5 GHz (or 20 pm). The resulting JSI has 16 times higher resolution with a 157 × 157 pixel grid.

3.4 Joint Spectral Intensity Results

For the simulation of the JSI for the different laser pulses, the dispersion relation from equation 3.6 was for $k_0 = 9.63 \times 10^6$ m^{-1}, $v_p = 7.02 \times 10^7$ m/s and $GVD = -6.03 \times 10^{-25}$ s^2/m. Using these parameters and the geometry of the SiNW waveguide, equation 2.22 was used to calculate the expected JSI for the two laser pulses. The resulting JSI distributions are shown in Fig. 3.12.

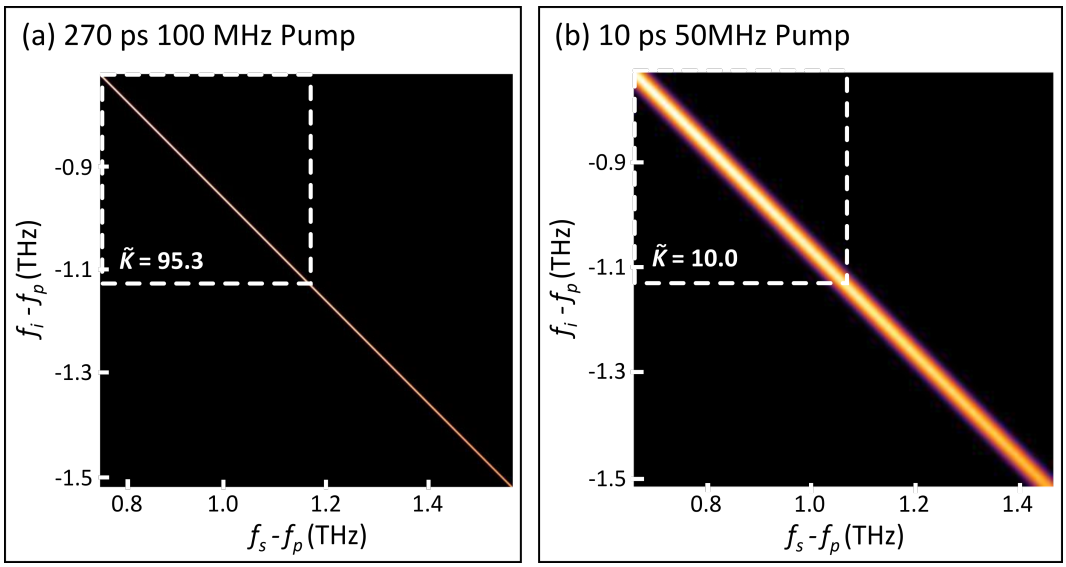

FIGURE 3.12. The scaled theoretically-calculated model for (a) the 270 ps and (b) 10 ps pump laser pulses, with dashed box representing the measured region.

As expected, for pulses increasing in duration towards quasi-continuous wave (CW), the high SNLB in Fig. 3.12 (a) indicates a more highly spectrally correlated state compared with Fig. 3.12 (b). This regime of very strong frequency correlations is particularly important in quantum information applications as many protocols relay on

time-frequency entanglement for use in, for example quantum cryptography and quantum computation. Note the slight curvature and decrease in brightness of the curves from top left to bottom right in the ideal modelled JSIs in Fig. 3.12 (a) and (b). As the JSI is a convolution of the pump profile and the phase matching function (recall equation 2.22), we would expect the JSI to decay to background if we continued to measure it beyond 1.135 THz from the central frequency of the pump.

Unlike some spontaneous FWM or spontaneous PDC processes where the generated signal and idler photons are phase-matched far from the pump, the SiNW dispersion does not allow for measurement of the whole JSI as the pump frequency lies in the centre (see Fig. 2.8). However in practice, this is not a serious restriction, since this band will also be inaccessible in any application of such source. This measurement is therefore concerned with an experimentally accessible portion of the JSI, over a tuning frequency range of 0.745-1.135 THz (5.94-9.15 nm) from the centre frequency of the pump, as shown in Fig. 3.12. The complete theoretical JSI was calculated and SVD was performed on that part of the spectrum accessible to our measurements.

Pump Pulse Duration	40 by 40 grid $\tilde{K}$	157 by 157 grid $\tilde{K}$	Ideal $\tilde{K}$
270 ps	39.0	83.5	95.3
10 ps	8.1	8.4	9.9

Table 3.1: Theoretically extracted SNLBs, $\tilde{K}$, for a 40 by 40, 157 by 157 and ideal JSIs, for the 270 ps 100 MHz and 10 ps 50 MHz laser pump pulses.

The SNLB associated with this experimentally accessible portion was used to quantify the accuracy of each measurement. However, the measured values of $\tilde{K}$ are affected by the available frequency resolution, as well as the noise in each class of experiment. To understand the impact of limited resolution, and thus separate this from the impact of noise in the experimental data, for each of the pump pulse lengths, the expected theoretical values of $\tilde{K}$ was calculated, at each of the available frequency resolution and a reference value at much finer resolution beyond which $\tilde{K}$ does not change in the 4th decimal place. Note that in our case, the combination of accessible frequency range and dispersion strength meant that no difference was found between the value of the SNLB, $\tilde{K}$, and the true Schmidt number, K, in the high resolution calculations. This of course would not be true in general.

The expected impact of limited resolution is shown in Table 3.1. It is clear that for the narrow-band width 270 ps pump source, the maximum observable value of $\tilde{K}$ is

significantly reduced from its ideal value. On the other hand, for the broadband 10 ps source, even the course resolution of 40×40 grid can represent a $\tilde{K}$ exceeding 80% of the ideal Schmidt number. The extent to which the measured values fall below these limits is a measure of the impact of noise of various types.

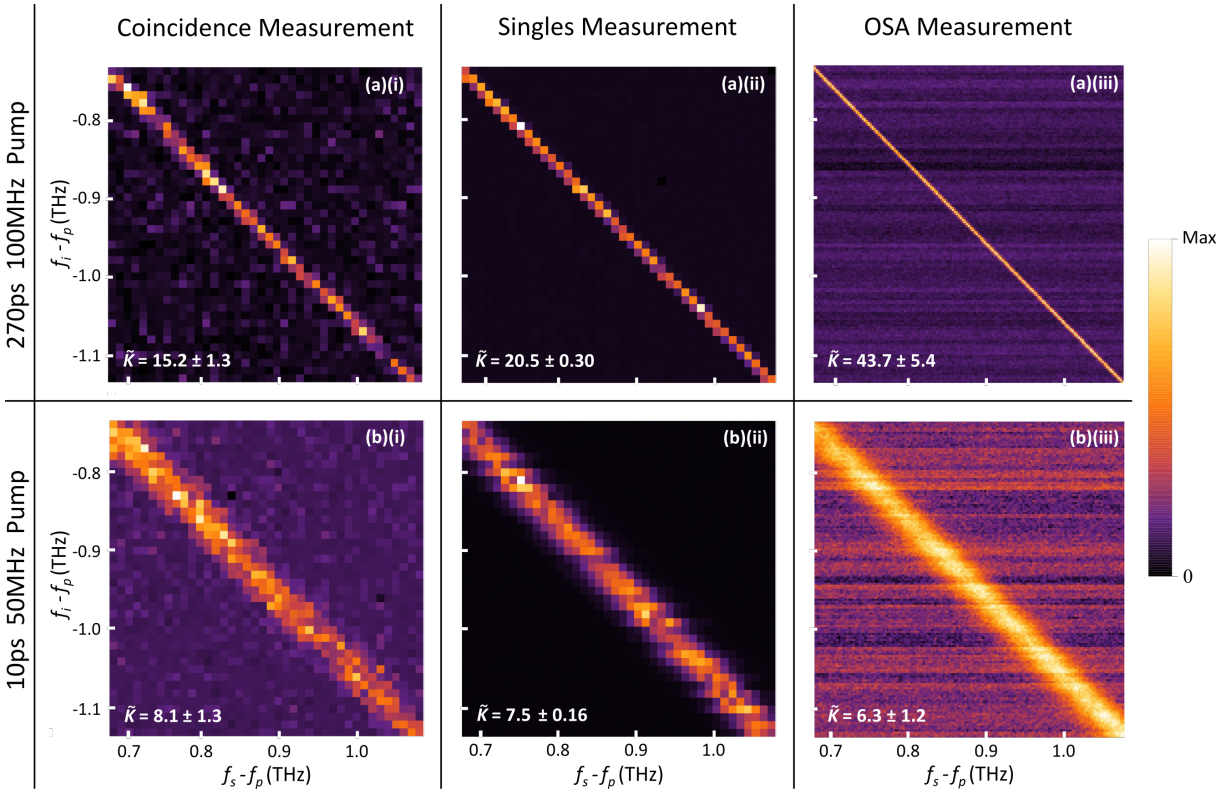

FIGURE 3.13. The results of the six JSI measurements, for (a) the 270 ps and (b) 10 ps pump laser pulses: (i) photon pair coincidence measurement, (ii) stimulated FWM singles-based measurement and (iii) stimulated FWM OSA measurement. The brightest pixel in each plot (Max of the colour bar) corresponds to: (a)(i) 105 coincidences, (b)(i) 105 coincidences, (a)(ii) 318,720 counts, (b)(ii) 182,210 counts, (a)(iii) 1716.7 nW/10 GHz, and (b)(iii) 464.1 nW/10 GHz. These maxima all have Poissonian error except those for (a)(iii) and (b)(iii) which have an inherent error from the OSA. SNLBs are shown for each plot with errors calculated from Monte Carlo simulations.

With the combination of the two laser pulses and the three detection methods, we measured a total of six partial JSIs. The three experimental JSI measurements are shown in Fig. 3.13(a) and (b) for the 270 ps and 10 ps pulses respectively, with their associated SNLBs, $\tilde{K}$, estimated by SVD and their respective errors estimated from

Monte Carlo simulations. These simulations re-sampled each point of each measured JSI from a Poissonian distribution to create 105 new Poissonian distributed JSIs for each measured JSI. Then the SNLB was calculated for each of the 105 new JSIs for each measurement, and the standard deviation of the distribution of the SNLBs were then used as the error in the SNLBs.

The total time taken to build up the 40 by 40 pixel grid (10 GHz resolution) coincidence JSI plots shown in Fig. 3.13(a)(i) and (b)(i) was approximately 36 hrs and 33 hrs respectively. During this time we continually adjusted the LCoSWS pass band for each channel across the whole JSI at a rate of 6 pixels per minute, summing the pixels from each scan until the largest number of recorded coincidence counts in any one pixel was 105 with a Poissonian error of 10. This repeated sampling process was designed to minimise the effect of slow fluctuations in laser power and waveguide couplings. Using this method for coincidence measurements, the high integration times can also be attributed to the LCoSWS rejecting most of the generated signal and idler photons that are not captured by pass band. As theoretically predicted, the broader spectral profile of the 10 ps laser source results in a broader anti-diagonal band, and thus a lower SNLB, for its associated JSI than that associated with the 270 ps source. As this is a spontaneous FWM measurement, the impact of accidental coincidences in JSI plots is large and contributes to a lower extracted SNLB than predicted.

The generated single photon measurements corresponding to the experimental setup in Fig. 3.11(a) are plotted in Fig. 3.13(a)(ii),(b)(ii). As stimulated FWM leads to a count rate at a single detector on the order of 105 s^{-1}, very low relative numbers of background singles are seen when scanning the LCoSWS band pass filter. The counts in the dark background region are only limited by dark counts from our detectors, which are on the order of 100 s^{-1}. In this case, a higher SNR in turn results in a higher SNLB being obtained when compared with the coincidence measurements, evident in the 270 ps pumped singles measurement in Fig. 3.13(a)(ii). However, a slightly lower SNLB was obtained for the 10 ps laser pulse in Fig. 3.13(b)(ii) compared with the corresponding coincidence measurement. This is caused by the non-uniform distribution of singles across the anti-diagonal band of the plot which occures as a result of small fluctuations in the laser powers, detector efficiency, and polarisation from scan to scan. Additionally, the 10 ps pumped coincidence value for the 40×40 grid ($\tilde{K} = 8.1$) provided the closest agreement to the expected value ($\tilde{K} = 9.9$) when compared with the singles-based measurement. Due to the high rate of stimulated FWM idler photon generation, the integration time for both pump measurements was limited only by the scanning speed of

the seed laser and the LCoSWS, as well as the speed of the electronic acquisition. Thus the fastest possible integration time for both measurements was only 1.5 hours. Still, moving to this singles-based measurement results in a significant decrease in the required integration time when compared to the coincidence measurement, while providing comparable SNLBs. The classical OSA measurements shown in Fig. 3.13(a)(iii),(b)(iii) were completed within 2 hours for each laser pulse width but with 16 times higher resolution, at the maximum resolution of 2.5 GHz. The horizontal streaks visible in both JSI plots are a result of the constant change in the noise floor of the OSA with every trace measurement. In theory, the streaks can be eliminated by averaging multiple traces for a fixed seed frequency, but not without increasing the total integration time of each JSI measurement. In principle, using this method we are able to measure the complete JSI profile of the SiNW, as the OSA is not saturated by the input pump at the powers used here.

3.4.1 Conclusions

I have presented measurements comparing JSIs from a $\chi^{(3)}$ nonlinear device, a SiNW, via three different experimental methods that can be used to characterise the correlations between generated photon pairs. This is achieved by employing both quantum correlation measurements and classical stimulated measurements, which makes use of the relationship between spontaneous FWM and stimulated FWM. For the stimulated FWM processes, we have shown two techniques, one that uses no further components than quantum correlations, other than a CW probe laser, and the other using a high resolution OSA. By successfully measuring the JSI in the quantum and classical regimes for two different laser pulses, we observed a direct change in the spectral correlation of the generated photon states, proving the versatility of our characterisation schemes. For the JSI measurements, we saw by switching from the quantum to classical measurements, we were able to increase the resolution from 10 GHz using the LCoSWS to 2.5 GHz using the OSA. However this also resulted in horizontal streaks in the JSI, a problem attributed to fluctuations in the noise floor of the OSA, and increased the relative error in the SNLB. In the future this could be overcome by using a lower noise OSA or limiting measurements to nonlinear devices with a higher FWM conversion efficiency as we would be operating further from the noise floor of the OSA.

As tabulated in table 3.1 By comparing the SNLBs calculated via SVD of our quantum and classical measurements with our ideal theoretical model, we conclude that the OSA provided the most accurate spectral correlation measurement (although half of

the predicted SNLB) for the long pump pulse. The measured spectral correlation for the short pump pulse via coincidence measurement provided us with the smallest deviation from the ideal model however, the measurement obtained via the OSA has a larger disagreement with the theory as a result of the horizontal streaks in the JSI measurement. Note that the stimulated FWM method provides the fastest measurement speed for a given resolution and thus the OSA measurement will consistently provide the highest resolution for future measurements of JSIs. Overall, the long pump pulse spectral correlation measurement provided us with the biggest discrepancy when compared to the ideal model, caused by the discretised JSI measurements having a limited resolution at the same scale as the pump spectral profile. Although not possible with the LCoSWS at this time, in theory the measurement resolution could be improved by reducing the LCoSWS programmable bandpass filter bandwidth. However, if we were able to reduce the LCoSWS filter bandwidth to the OSA resolution of 2.5 GHz for measurement in the coincidence counting regime, the measurement time would increase by a factor of 16, meaning a JSI measurement would take approximately 24 days of continuous measurements.

In the next chapter, we will investigate a novel method that again uses stimulated FWM to for the first time measure the JSA of photon pairs for a full quantum tomography measurement. We will use this novel technique to measure the JSA measurement of another but identical SiNW and and apply this technique to a HNLF.

CHAPTER 4

PHASE-SENSITIVE JOINT SPECTRAL AMPLITUDE MEASUREMENT

In the last chapter, we introduced SET, as an alternative method of JSI measurement in the classical regime. We compared the traditional based coincidence measurement of the photon pairs generated via spontaneous FWM with stimulated FWM and saw excellent agreement between the two. We concluded that stimulated based measurement of the JSI is the best method for a fast and high resolution characterisation of photon pair sources that requires no single photon detectors but only an of the shelf OSA. In this chapter, we extend this classical method of measurement of the JSI, to for the first time, measure the phase relationship between the signal and idler photon pairs. We use a novel technique that is fully stabilised to perform full quantum tomogrpahy of the photon pairs by measuring the JSA. In this chapter we will

- Present a novel method of measuring the JSA in the classical regime using phase sensitive amplification and SET.
- Perform comparison of JSI and JSA measurements and what a JSA can reveal that is usually hidden in a JSI measurement for a silicon nanowire.
- Observe hidden artifacts of sinc side lobes as a result of phase-matching, that are not visible in a JSI measurement.

This chapter is based on the following publication:

I. Jizan, B. Bell, A.C. Bedoya, C. Xiong and B.J. Eggleton, "Phase-Sensitive Quantum Tomography of Joint Spectrum Photon Pairs.", *In preparation*, (2016).

4.1 The Joint Spectral Amplitude

As explained in the previous chapters, the modulus square of the JSA, the JSI can be measured directly using a coincidence counting setup with single photon detectors using the temporal dispersion method or spatial separation method involving narrow filters at the two frequencies of interest. However mapping out the JSI can be very time consuming and tends to suffer from low-resolution plots as the measurement takes place in the single photon regime. Furthermore this coincidence measurement of the JSI is an intensity based measurement that results in the loss of phase information that is necessary for complete characterisation of the photon pairs, requiring the measurement of the JSA. Although not impossible, obtaining the full phase sensitive information of photon pairs in the single photon regime is experimentally very challenging and requires what is referred to homodyne detection setup.

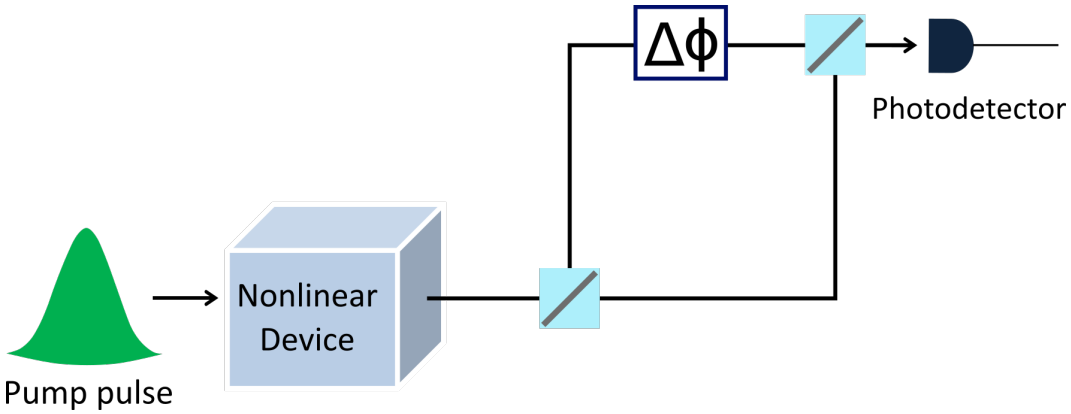

FIGURE 4.1. Schematics of a homodyne detection setup where the output signal is split and interfered with itself.

In optics, a homodyne detection is a detection setup where an input signal is mixed with some other wave, that is often known as a local oscillator, in some nonlinear device where the resulting mixing product is then detected. A variant of this detection method is where the local oscillator is derived from the same source of the input signal. A simplified version of such homodyne detection setup is shown in Fig. 4.1. In the context of homodyne detection in the single photon regime, it requires the interference of one photon with

the partner photon. This method has been successfully implemented for phase-space tomography of a quantum process [68].

However, standard homodyne detection setup for photon pairs measures in the single photon regime and neglects any spectral correlations. Although not impossible, phase sensitive measurement of spectrally correlated photon pairs requires a unique homodyne detection setup that requires the interference of the generated photon with a local oscillator that is also in the single photon level. As such, phase sensitive measurement of spectrally correlated photon pairs in the quantum regime is very challenging and involves a large effort of data processing techniques [58].

The recently proposed method of SET, where the FWM or PDC is stimulated with a seed laser at one of the two frequencies, allowed for a new method of JSI measurement with unprecedented resolution and accuracy as we saw in the previous chapter. Although SET can be thought of as an entirely classical process, the response function of the nonlinear media for the spontaneous and stimulated process are mathematically identical and therefore the intensity of emitted light at the unseeded frequency is proportional to the JSI. Mathematically, we can express this by

$$A_{SET}(\omega_i, \omega_s) = A^*_{seed} \times A(\omega_i, \omega_s), \tag{4.1}$$

where $A_{SET}(\omega_s, \omega_i)$ is the stimulated emission amplitude, A^*_{seed} is the conjugate of the seed field input amplitude and $A(\omega_i, \omega_s)$ is the joint spectral amplitude defined in equation 2.22. As discussed in Chapter 3, this therefore avoids the need of specialised detectors and coincidence counting, as it is only necessary to measure the intensity at one frequency, that is well above the single photon level. This allows one to make a fast, high resolution classical characterisation of a quantum device using standard photodetectors or OSAs.

The light emitted in SET already carries the necessary phase as well as intensity information, requiring only a phase sensitive detection. In this chapter, I will show that phase sensitive amplification (PSA), with input light at both frequencies is sufficient to measure the complete JSA. The stimulated mission $A_{SET}(\omega_s, \omega_i)$ interferes constructively or constructively with input light, which acts as a phase reference. We apply this method of using SET in combination with PSA to two $\chi^{(3)}$ devices; a different integrated SiNW and a HNLF. Using the SiNW, we show that if a frequency chirp is added to the pump laser pulse, the JSA closely reflects this change and thus increasing the degree of entanglement generated by the source while no change is seen in the JSI. With the HNLF, we observe the sinc function related to the phase-matching of the FWM and

find that our method allows us to detect small features in the JSA with unprecedented accuracy.

4.2 Measurement of the Joint Spectral Amplitude

Using stimulated FWM to measure the JSI requires a classical seed field in the signal or idler band in addition to the pump pulse where the generated field is then detected to plot the JSI. However, one can measure the JSA by measuring the phase of the generated field by employing a homodyne detection technique. However, unlike the previously mentioned homodyne detection setup in the single photon regime, this homodyne detection setup require the classical interference of the generated field a classical local oscillator.

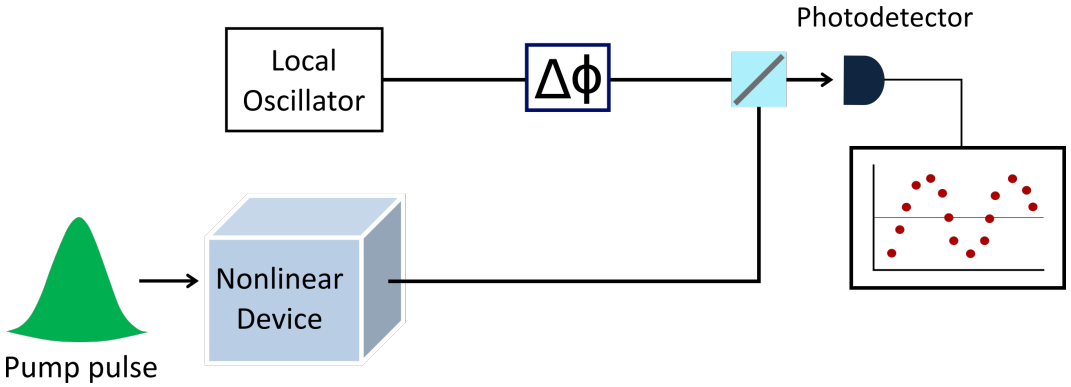

FIGURE 4.2. An illustration of a homodyne detection setup where the generated field via stimulated FWM is combined with a local oscillator before detection with a photodetector.

Fig. 4.2 shows a setup where homodyne detection allows for phase sensitive measurement of the JSA. By combining the generated field with a local oscillator, one is then able to measure the relative phase of the generated field by varying the phase of the local oscillator. Of course one is able to instead vary the phase of the generated field instead of the local oscillator. As the generated field and local oscillators combine, the phase change in the local oscillator will result in constructive and destructive interference when detected and thus allowing for complete measurement of the JSA. Although it is experimentally doable, performing this type of measurement at multiple frequencies to build a JSA will be experimentally challenging. This type of phase-sensitive measurement will suffer from phase instability and mode overlap between the generated field and local oscillator and therefore will result in large experimental effort, which is not desirable in the field of quantum photonics.

A more effective and convenient method of measuring the JSA is to perform phase sensitive measurement in the nonlinear device where all input lights follow a common path, ensuring a high degree of phase-stability and perfect mode overlap. This type of phase sensitive measurement in the nonlinear device is known as PSA and plays an important role in signal processing in laser communication systems [69]. In a nutshell, PSA is a amplification process whose gain depends on the input phase. In $\chi^{(3)}$ nonlinear media, the generated field in stimulated FWM depends on the relative input phase of the seed or pump fields.

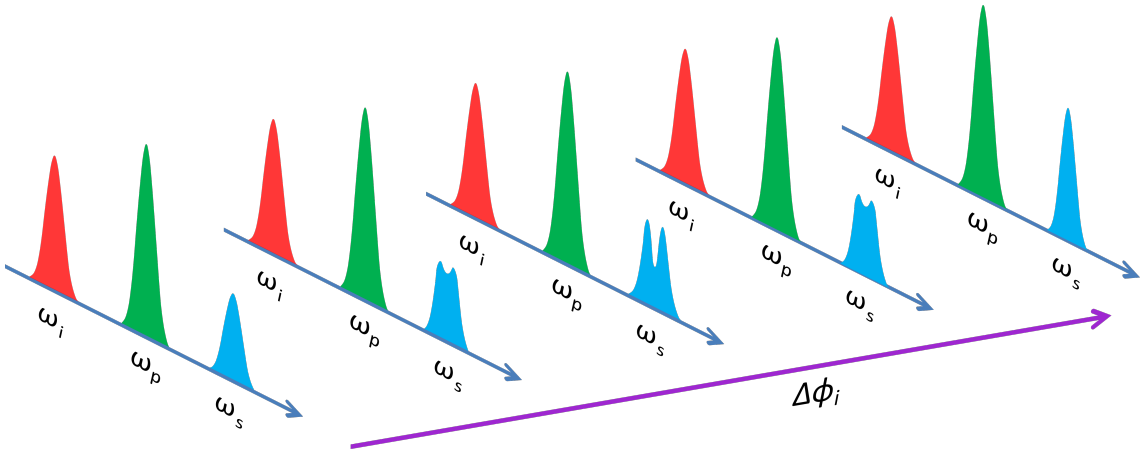

FIGURE 4.3. An illustration of PSA where the generated field via stimulated FWM is interfered with a reference field resulting in constructive or deconstructive interference as the phase of the seed field is varied.

Referring to Fig. 4.3, by inputting three fields; seed (ω_i), pump (ω_p) and a reference field (ω_s) into the nonlinear device, the generated field via FWM in the signal frequency (ω_s) will interfere with the reference field that results in constructive or deconstructive interference, that is dependent on the input phase of the seed field. Thus by combining PSA and SET, we are able to perform phase-sensitive tomography and obtain the full JSA of the source by measuring the spectrum of the reference beam for different phase shifts in the seed field.

In this work, we apply this method to two $\chi^{(3)}$ nonlinear devices; an integrated SiNW and a HNLF. Using the SiNW, I will show that if a frequency chirp is added to the pump laser pulse, the JSA closely reflects this change and see an increase in the degree of spectral entanglement generated by the source while no change is seen the JSI. With the HNLF, we observe the sinc function related to the phase-matching of FWM, and find that our method allows us to detect small features in the JSA with unprecedented accuracy.

4.3 The Experimental Setup

We employed a single broadband laser to provide the three pulses necessary for a PSA JSA measurement; a pump pulse, a seed pulse to stimulate the FWM and a broadband phase reference pulse covering the stimulated emission frequencies of interest. Fig. 4.4 shows the experimental setup.

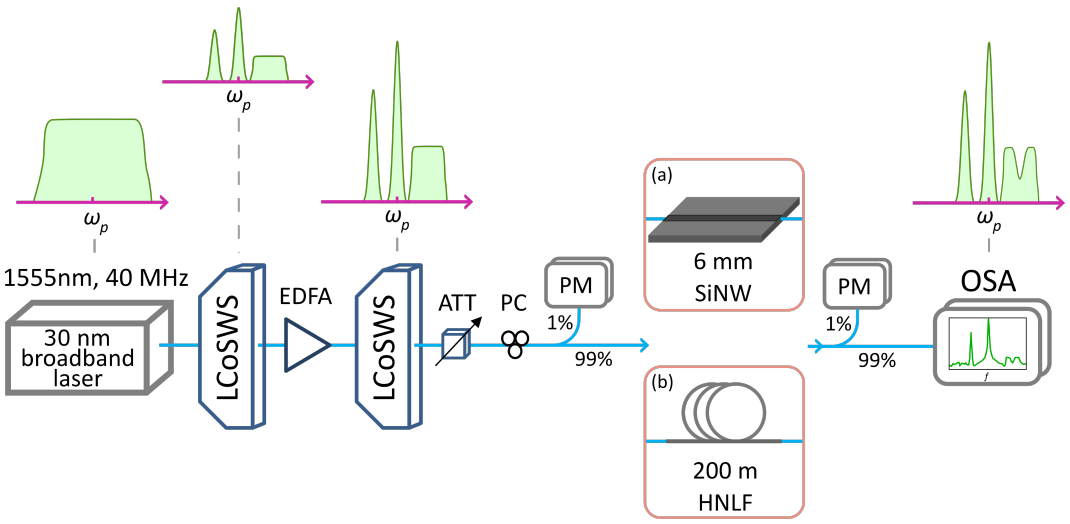

FIGURE 4.4. Schematics of the experimental setups of JSA measurement for 6 mm silicon nanowire (SiNW) and a 200 m highly nonlinear fiber (HNLF). See text for detailed description.

A mode-locked laser produces pulses of 30 nm bandwidth centred at 1555 nm, with 40 MHz repetition rate. The pulses are then passed through a LCoSWS as used in the previous chapter, to slice the broadband laser into the pump, seed and reference pulses. Although not mentioned in the previous chapter, but as well as allowing arbitrary filter shapes, the LCoSWS can apply any phase shift as a function of wavelength to generate group delay or dispersion for a pulse. A Gaussian pump is defined near the centre of the spectrum. The seed is scanned over the available wavelengths longer than the pump to map out the JSA. The seed has a Gaussian spectrum with 10 GHz bandwidth, the minimum allowed by the LCoSWS. Ideally, the seed should be a delta function in wavelength, however this finite bandwidth of 10 GHz limits resolution of the JSA with respect to the seed wavelength. The broadband reference light is positioned to the short wavelength side of the pump with a bandwidth greater than 1 THz.

The sliced pulses are passed though an EDFA, to amplify the three pulses. To avoid FWM inside the EDFA, the pump and the reference light were delayed by +15 ps and

-15 ps with respect to the seed pulse using the LCoSWS. Additionally, the reference pulse and the seed were attenuated by 15 dB and 6 dB respectively. Then, a second LCoSWS was used to delay the pump and reference light by -15ps and +15ps, bringing them back into overlap with the seed, and vary the relative phase of the seed pulse. The second LCoSWS also attenuated the seed beam by another 6 dB while simultaneously blocking any amplified spontaneous emission noise from the EDFA. When required, the second LCoSWS was also used to induce a chirp in the pump frequency with a chirp rate of approximately 1.1 GHz/ps.

Before the nonlinear device, a variable attenuator (ATT) was used to tune the input power, and a polarisation controller (PC) was used to control the polarisation of the input pulses. The two $\chi^{(3)}$ nonlinear devices that were used were a SiNW and HNLF (Fig. 2 (a) and (b) respectively). The SiNW is a 6 mm long silicon-on-insulator waveguide, 220 nm high by 460 nm wide, with an effective nonlinearity of approximately γ = 236 $W^{-1}m^{-1}$, and grating couplers at the input and output. Single mode fibers were glued to the input and output, resulting in a relatively high insertion loss of around 19 dB, but ensuring that the coupling was stable over the course of the measurement. The HNLF is a 200 m dispersion engineered fibre with an effective nonlinearity of approximately γ = 10 $W^{-1}m^{-1}$. The combined input and output losses were measured to be approximately 0.5 dB. The input and output powers from the nonlinear devices were monitored using two 99:1% couplers, with the 1% being sent to a power meter (PM). Finally, an OSA was used to measure the PSA output spectrum with a resolution of 30 pm.

For the JSA measurement of the SiNW, the seed field was scanned from 1557-1566 nm with a resolution of 5 GHz. For the JSA measurement of the HNLF, the seed field was brought much closer to the pump with a scanning range from 1555-1568 nm for the same step resolution of 5 GHz. Note that unlike some nonlinear devices where spontaneous PDC and FWM are phase-matched far from the pump, our SiNW and HNLF does not allow for measurement of the whole JSA as the pump frequency is at the centre as in Chapter 3. Therefore our measurement is concerned with the accessible portion of the JSA that is useful in any application of such source. The measurements were completed within 17 hours, limited only by the scanning speed of the seed pulse from LCoWS and scanning speed of the OSA.

4.4 Joint Spectral Intensity Results

The JSA measurement for each seed wavelength consisted of four scans of the spectrum corresponding to four phase-shifts applied to the seed pulse: θ = 0, $\frac{\pi}{2}$, π, $\frac{3\pi}{2}$. The change in θ resulted in constructive and deconstructive between the stimulated emission and the reference light, with the resulting intensity varying according to

$$|A_{seed}F(\omega_s,\omega_i)|^2+|A_{ref}|^2+|A_seed\times A_{ref}|Re(F(\omega_s,\omega_i)cos\theta+|A_{ref}\times A_{seed}|Im(F(\omega_s,\omega_i))sin\theta. \tag{4.2}$$

Taking the difference between two scans removes the first two (phase-insensitive) terms, and any constant background, leaving the phase-sensitive terms which are proportional to the real and imaginary parts of the JSA. In particular, the real and imaginary part of the JSA were obtained by subtracting the θ = 0, π scans and the θ = $\frac{\pi}{2}$, $\frac{3\pi}{2}$ scans respectively. For each scan, the seed pulse was also scanned to normalise out the dependence on $|A_{seed}|$, and one scan of the reference spectrum with the seed switched off was used to normalise out the dependence on $|A_{ref}|$.

4.4.1 Silicon Nanowire: Un-Chirped Pump

Fig. 4.5(a) (i), (ii), and (iii) contain the result, showing respectively the JSI calculated from the JSA, the real part of the JSA, and the imaginary part for the frequency un-chirped pump. For comparison, Fig. 3(b) shows the corresponding results from a theoretical model, calculated as in Chapter 3.

The experimental JSI shows good agreement with the model, with the FWM contained in a line at -45° such that signal and idler remain equidistant around the pump, as required by energy-matching, and the width of this line reflects the bandwidth of the pump. The SiNW is short enough that phase-matching does not affect the JSI over this range. However, the real and imaginary parts of the experimental JSA show oscillations along the -45° line, while the model predicts a constant phase. This change in phase with frequency is unlikely to come from the short SiNW, and probably is already present in the input fields, either because the phase is not constant over the spectrum of the initial laser pulse, or because of dispersive effects in the EDFA. This could lead to an arbitrary variation in the phase of the reference light with frequency, or in a change in the seed phase as it is scanned. Note that these effects lead to separable changes to the phase and do not affect the level of entanglement in the JSA. In principle, the LCoSWS could be used to pre-compensate for this phase variation in the input fields.

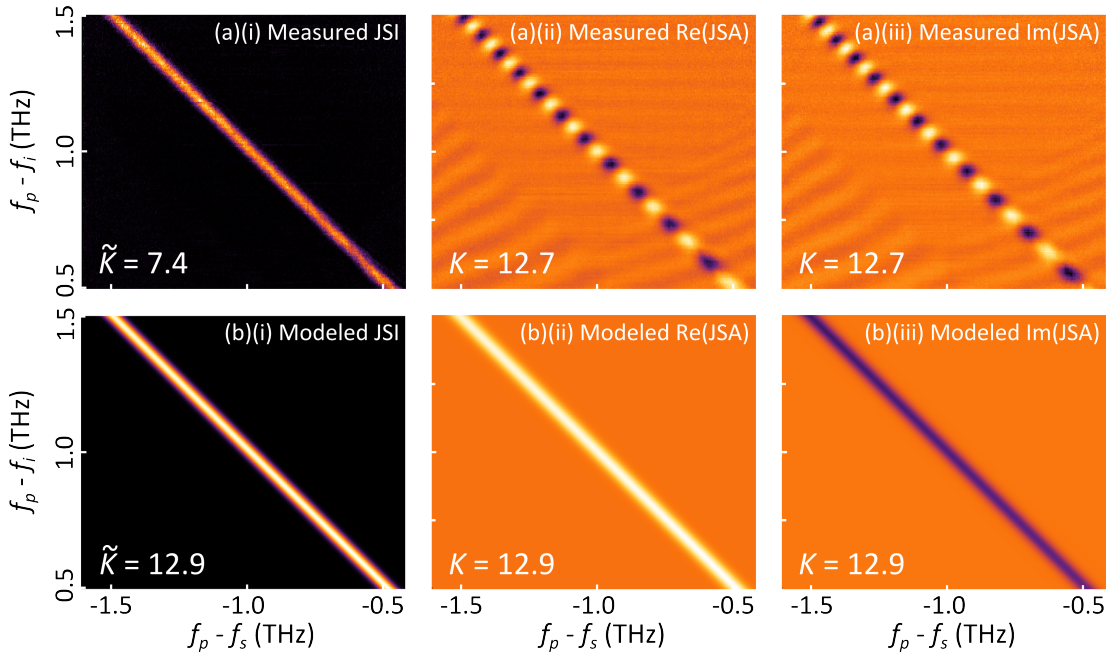

FIGURE 4.5. The (a) measured and (b) theoretically modelled plots of (i) JSIs, and normalised plots of (ii) real and (iii) imaginary parts of the JSA of SiNW for a frequency un-chirped pump.

In Fig. 4.5, the theoretical model predicts $K = \tilde{K} = 12.9$ for the JSA - since the predicted phase is flat over the JSA, there are no additional phase correlations and the Schmidt number is equal to the lower limit. However, for the experimental result $\tilde{K} = 7.4$. Schmidt numbers derived from experimental JSIs often underestimate the value, because the presence of a flat noise-floor extending over the measured area reduces the effect of the correlations. On the other hand, the experimental value $K = 12.7$ is in good agreement with the model since the background noise in the JSA is centred about zero, rather than being necessarily positive as in the JSI as it has less of an effect on the degree of correlation.

4.4.2 Silicon Nanowire: Chirped Pump

By then introducing a frequency a frequency chirp to the pump pulse using the second LCoSWS, we expect to create correlated phase changes in the JSA, leading to an increase in K but no change in $\tilde{K}$. In Fig. 4.6, we have plotted the measured and theoretically modelled JSI and JSA of the SiNW with the chirped pump. The JSI plots show little change compared to the un-chirped case in Fig. 4.5, except for an increase in experimental

noise associated with applying a large chirp, which decreases the experimental SNLB to $\tilde{K}$ = 6.7.

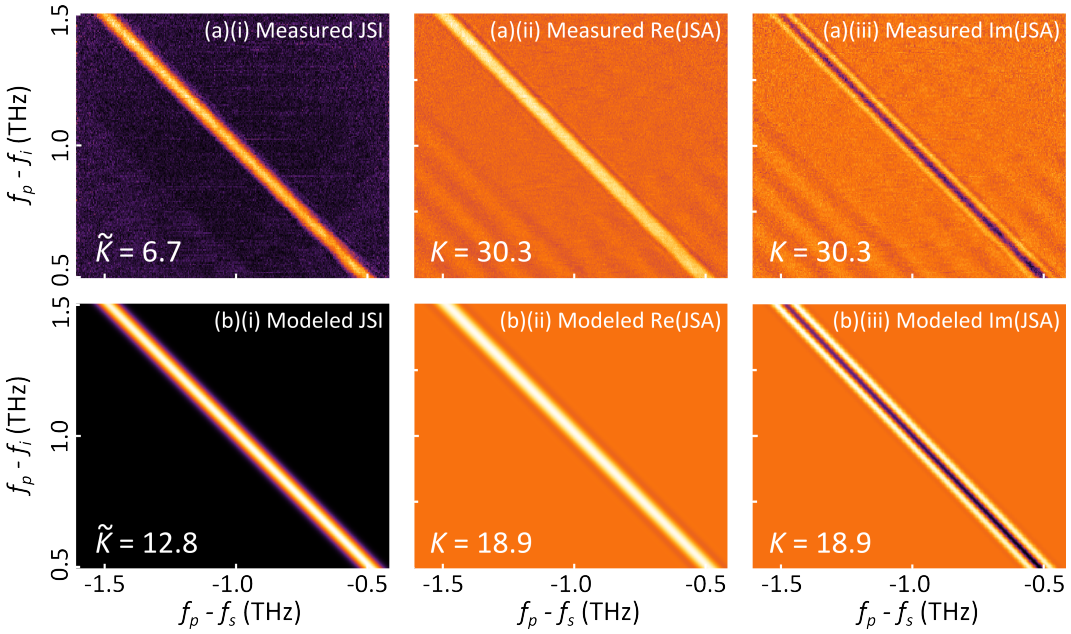

FIGURE 4.6. The (a) measured and (b) theoretically modelled plots of (i) JSIs, and normalised plots of (ii) real and (iii) imaginary parts of the JSA of SiNW for a frequency chirped pump.

In the JSA plots, the phase oscillations associated with the input fields have been removed, by subtracting the phase of the un-chirped JSA, allowing the effects of the chirp to be seen clearly. The phase oscillates across the narrow width of the JSA at +45° , which is particularly apparent in the imaginary part, with good qualitative agreement between the experiment and the model. The Schmidt numbers of the measured and modelled JSAs are K = 30.3 and K = 18.9 respectively. As predicted, a higher Schmidt number is obtained for the JSA with a chirped pump pulse. However, in this case, the experimental noise leads to a larger Schmidt number than predicted by the model. The noise appears to have the opposite effect here compared to in the JSIs where sufficient noise in the JSA can introduce additional correlations. This may be exacerbated here by the appearance of diagonal ripples in the phase of the noise, for instance in the bottom left of Fig. 4.5(a) (ii) and (iii), which gives the appearance of phase correlation. Since no PSA should occur in these areas, this probably originates from imperfections in the LCoSWS, for instance if the attenuation of noise from the EDFA varies in a systematic manner when the phase, θ, is adjusted.

4.4.3 Highly Nonlinear Fibre: Un-Chirped Pump

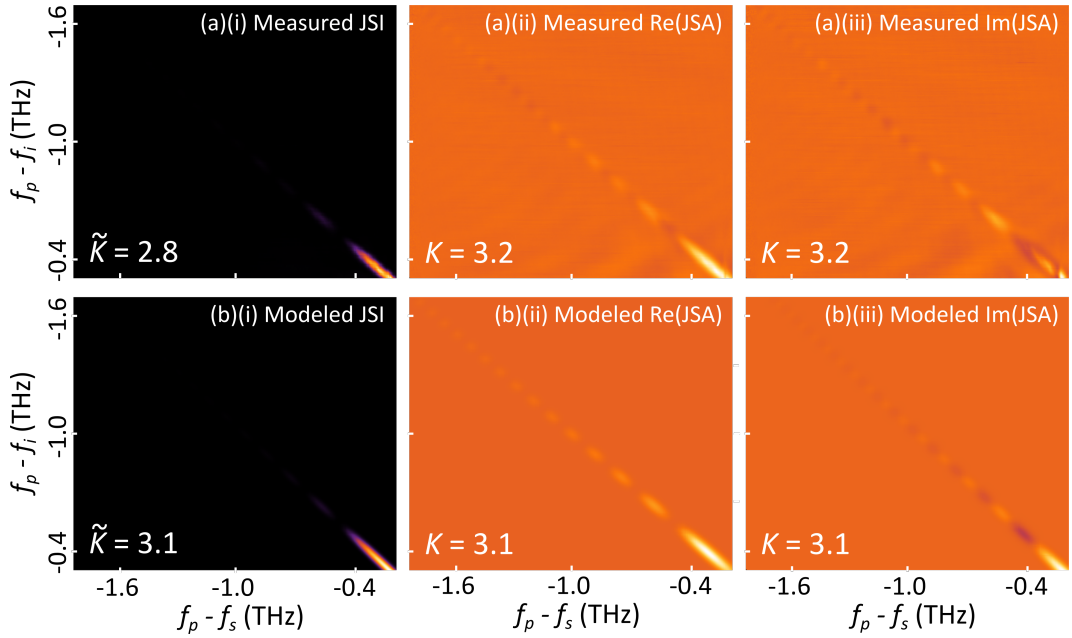

FIGURE 4.7. The (a) measured and (b) theoretically modelled plots of (i) JSIs, and normalised plots of (ii) real and (iii) imaginary parts of the JSA of HNLF for a frequency un-chirped pump.

Fig. 4.7 shows the experimental and modeled JSIs and the real and imaginary parts of the JSA for the HNLF. Unlike the SiNW, the phase mismatch of the FWM has a significant effect here, resulting in oscillations and a decrease in intensity as the signal and idler are moved away from the pump, following a sinc profile function. The measured results here show a better signal to noise ratio than for the SiNW, due to the lower insertion loss of the HNLF. In Fig. 4.7(a)(i) and (b)(i), the JSI shows the main peak of the function and the first oscillation can just be seen. In the measured and modelled plots of the JSA, the oscillations can be seen extending across the measured region, demonstrating the sensitivity of our measurement to very small features. The lower bound Schmidt number for the HNLF JSI was calculated to be $\tilde{K}$ = 2.8 from the ideal case of $\tilde{K}$ = 3.1. The Schmidt number of the measured and modelled JSAs were calculated to be K = 3.2 and K = 3.1 respectively, showing good agreement.

4.5 Conclusions

In conclusion, I have presented classical characterisations of the JSAs of photon-pairs generated by two $\chi^{(3)}$ nonlinear devices, a SiNW and HNLF, via a novel measurement technique that can be used for full phase-sensitive tomography of photon pair sources. This is achieved by combining SET with PSA for a coherent and phase-stable detection. By measuring the JSA of the SiNW for a frequency chirped and un-chirped pump, we are able to observe a corresponding change in the JSA that would be hidden in standard JSI measurements. The degree of correlation, quantified by the Schmidt number, increases as expected for the chirped pump, though the increase is larger than predicted by theory. This highlights an apparent difference between Schmidt numbers calculated from a JSI or a JSA and signifies the importance of measuring the JSA instead of the JSI. In the former case, experimental noise tends to decrease the Schmidt number, whereas in the latter noise tends to increase it. For the HNLF, we observe the characteristic sinc profile function dependence on phase mismatch, and find that the direct measurement of the JSA has excellent sensitivity to small features compared to measurements of the JSI.

CHAPTER 5

SUMMARY AND CONCLUSIONS

In this thesis, I provided an quick overview of the non-intuitive behaviour of quantum mechanics such as quantum interference and how it has transformed the field of communication and computing. I discussed the specific advantages of using single photons as our quantum system compared to other platforms due to their well characterised states, and their weak interaction with matter. Therefore photons are prime candidates for transmitting information through existing optical fibre networks. However, as discussed in Chapter 2, this low weak interaction also posses difficulty in photon-photon interaction, a necessary requirement for quantum gate operations in quantum optical technologies. However quantum photonics emerged as a breakthrough solution, first proposed in 2001 via the KLM scheme that uses linear optics and photon interference for efficient single photon-photon interaction. The non-classical quantum interference between photons was discussed in detail for use in quantum circuits. The possible methods for generating single photons using an atom-like source, attenuated laser and nonlinear media were examined. From this, the coincidence-to-accidental, an important measurement of the photon statistics of a photon pair source was also introduced. A brief history of nonlinear optics and the theory of four-wave mixing in $\chi^{(3)}$ nonlinear media that produce spectrally correlated photons was explored. Subsequently, an overview of $\chi^{(3)}$ nonlinear devices such as silicon nanowire and highly nonlinear fibre that fully satisfy the energy and phase-matching requirements and thus creating high spectrally entangled photons pairs were also examined. Common method of characterising spectral correlation via coincidence-based measurement of the JSI using spatial

and temporal mode separation method and their limitations where discussed in details. To address the limitations with coincidence measurement of the JSI, I introduced SET where an additional seed filed is used to stimulate the generation of photons with much higher efficiency.

We applied the the SET method to a SiNW and compared the obtained JSI with the JSI obtained through coincidence based spatial mode separation of the photon pairs. This was done so by making use of the relationship between spontaneous FWM and stimulated FWM. For the stimulated FWM process, we have shown that it uses no detection components other than an OSA which provided the fastest measurement speed for a given resolution and most accurate spectral correlation measurement. By successfully measuring the JSI in the quantum and classical regimes for two different laser pulses, we observed a direct change in the spectral correlation of the generated photon states, proving the versatility of the characterisation technique. We have also presented the first measurement of the JSA (the square root of the JSI) that contains the phase information of photon pairs, using a novel measurement technique that uses SET and PSA. We performed these JSA measurements on two $\chi^{(3)}$ nonlinear devices, a SiNW and HNLF. By measuring the JSA of the SiNW for a frequency chirped and un-chirped pump, we are able to observe a direct change in the JSA that would otherwise be hidden in standard JSI measurements. JSA measurement of the HNLF revealed sinc profile lobes as the result of phase-matching that are not normally visible in standard JSI measurements.

In the future, the methods I presented in this thesis can be applied to other integrated pair generation devices including ring resonators, and slow-light photonic crystals [43–48]. Furthermore, the novel technique of measuring the JSA can be applied to any $\chi^{(3)}$ or $\chi^{(2)}$ source of photon pairs, though it requires a coherent source of light at the pump, signal, and idler frequencies of interest, which allows PSA to be carried out. This may be useful in future attempts to optimise nonlinear devices for pair-photon generation when either a high degree of spectral entanglement or the absence of spectral entanglement are desirable. In conclusion, the methods presented here are of substantial importance for the characterisation of spectrally correlated photon states, particularly for non-linear devices that require fast, reliable and phase sensitive measurements, and when large numbers of devices must be characterised for use in future quantum photonic technologies.

APPENDIX A

APPENDIX: PUBLICATION LIST

Publications included in this thesis

1. **I. Jizan**, L.G. Helt, C. Xiong, M.J. Collins, D.Y. Choi, C.J. Chae, M. Liscidini, M.J. Steel, B.J. Eggleton and A.S. Clark, "Bi-photon spectral correlation measurements from a silicon nanowire in the quantum and classical regimes.", *Scientific reports*, **5**, 12557, (2015).

2. **I. Jizan**, B. Bell, A.C. Bedoya, C. Xiong and B.J. Eggleton, "Phase-Sensitive Quantum Tomography of Joint Spectrum Photon Pairs.", *In preparation*, (2016).

Other publications

1. **I. Jizan**, A.S. Clark,L.G. Helt, M.J. Collins, E. M*ä*gi, C. Xiong, M.J. Steel and B.J. Eggleton, "High-resolution measurement of spectral quantum correlations in the telecommunication band.", *Optics Communications*, **327**, 45-48, (2014).

2. X. Zhang, **I. Jizan**, J. He, A.S. Clark, D.Y. Choi, C.J. Chae, B.J. Eggleton and C. Xiong, "Enhancing the heralded single-photon rate from a silicon nanowire by time and wavelength division multiplexing pump pulses.", *Optics letters*, **40**, 2489-2492, (2015).

BIBLIOGRAPHY

[1] Richard P Feynman.
Quantum mechanical computers.
Foundations of physics, 16(6):507–531, 1986.

[2] Andrew Steane.
Quantum computing.
Reports on Progress in Physics, 61(2):117, 1998.

[3] L-M Duan, MD Lukin, J Ignacio Cirac, and Peter Zoller.
Long-distance quantum communication with atomic ensembles and linear optics.
Nature, 414(6862):413–418, 2001.

[4] GJ Milburn.
Quantum optical fredkin gate.
Physical Review Letters, 62(18):2124, 1989.

[5] Emanuel Knill, Raymond Laflamme, and Gerald J Milburn.
A scheme for efficient quantum computation with linear optics.
nature, 409(6816):46–52, 2001.

[6] Jeremy L O'Brien.
Optical quantum computing.
Science, 318(5856):1567–1570, 2007.

[7] Jeremy L O'Brien, Akira Furusawa, and Jelena Vučković.
Photonic quantum technologies.
Nature Photonics, 3(12):687–695, 2009.

[8] Nicolas Gisin and Rob Thew.
Quantum communication.
Nature Photonics, 1(3):165–171, 2007.

[9] David J Wineland, M Barrett, J Britton, J Chiaverini, B DeMarco, WM Itano, B Jelenković, C Langer, D Leibfried, V Meyer, et al.
Quantum information processing with trapped ions.
Philosophical Transactions of the Royal Society of London A: Mathematical, Physical and Engineering Sciences, 361(1808):1349–1361, 2003.

[10] Rutger Vrijen, Eli Yablonovitch, Kang Wang, Hong Wen Jiang, Alex Balandin, Vwani Roychowdhury, Tal Mor, and David DiVincenzo.
Electron-spin-resonance transistors for quantum computing in silicon-germanium heterostructures.
Physical Review A, 62(1):012306, 2000.

[11] Lev B Ioffe, Vadim B Geshkenbein, Mikhail V Feigel'Man, Alban L Fauchere, and Gianni Blatter.
Environmentally decoupled sds-wave josephson junctions for quantum computing.
Nature, 398(6729):679–681, 1999.

[12] Pieter Kok, William J Munro, Kae Nemoto, Timothy C Ralph, Jonathan P Dowling, and Gerard J Milburn.
Linear optical quantum computing with photonic qubits.
Reviews of Modern Physics, 79(1):135, 2007.

[13] Isaac L Chuang and Yoshihisa Yamamoto.
Simple quantum computer.
Physical Review A, 52(5):3489, 1995.

[14] Qi A Turchette, CJ Hood, W Lange, HJKH Mabuchi, and H Jerey Kimble.
Measurement of conditional phase shifts for quantum logic.
Physical Review Letters, 75(25):4710, 1995.

[15] H Schmidt and A Imamoglu.
Giant kerr nonlinearities obtained by electromagnetically induced transparency.
Optics letters, 21(23):1936–1938, 1996.

[16] Michael A Nielsen and Isaac L Chuang.
Quantum computation and quantum information.
Cambridge university press, 2010.

[17] CK Hong, ZY Ou, and Leonard Mandel.

Measurement of subpicosecond time intervals between two photons by interference.
Physical Review Letters, 59(18):2044, 1987.

[18] Charles Santori, David Fattal, Jelena Vučković, Glenn S Solomon, and Yoshihisa Yamamoto.
Indistinguishable photons from a single-photon device.
Nature, 419(6907):594–597, 2002.

[19] GD Fuchs, Guido Burkard, PV Klimov, and DD Awschalom.
A quantum memory intrinsic to single nitrogen-vacancy centres in diamond.
Nature Physics, 7(10):789–793, 2011.

[20] Juan I Cirac and Peter Zoller.
Quantum computations with cold trapped ions.
Physical review letters, 74(20):4091, 1995.

[21] C Ospelkaus, U Warring, Y Colombe, KR Brown, JM Amini, D Leibfried, and DJ Wineland.
Microwave quantum logic gates for trapped ions.
Nature, 476(7359):181–184, 2011.

[22] Charles H Bennett, Gilles Brassard, Claude Crépeau, Richard Jozsa, Asher Peres, and William K Wootters.
Teleporting an unknown quantum state via dual classical and einstein-podolsky-rosen channels.
Physical review letters, 70(13):1895, 1993.

[23] Qin Wang, Wei Chen, Guilherme Xavier, Marcin Swillo, Tao Zhang, Sebastien Sauge, Maria Tengner, Zheng-Fu Han, Guang-Can Guo, and Anders Karlsson.
Experimental decoy-state quantum key distribution with a sub-poissionian heralded single-photon source.
Physical review letters, 100(9):090501, 2008.

[24] Peter J Mosley, Jeff S Lundeen, Brian J Smith, Piotr Wasylczyk, Alfred B U,ÄôRen, Christine Silberhorn, and Ian A Walmsley.
Heralded generation of ultrafast single photons in pure quantum states.
Physical Review Letters, 100(13):133601, 2008.

[25] Matthew J Collins, Chunle Xiong, Isabella H Rey, Trung D Vo, Jiakun He, Shayan Shahnia, Christopher Reardon, Thomas F Krauss, MJ Steel, Alex S Clark, et al.

Integrated spatial multiplexing of heralded single-photon sources.
Nature communications, 4, 2013.

[26] Hiroki Takesue and Kaoru Shimizu.
Effects of multiple pairs on visibility measurements of entangled photons generated by spontaneous parametric processes.
Optics Communications, 283(2):276–287, 2010.

[27] PA Franken, AE Hill, CW el Peters, and G Weinreich.
Generation of optical harmonics.
Physical Review Letters, 7(4):118, 1961.

[28] RL Carman, RY Chiao, and PL Kelley.
Observation of degenerate stimulated four-photon interaction and four-wave parametric amplification.
Physical Review Letters, 17(26):1281, 1966.

[29] David C Burnham and Donald L Weinberg.
Observation of simultaneity in parametric production of optical photon pairs.
Physical Review Letters, 25(2):84, 1970.

[30] Alain Aspect, Jean Dalibard, and Gérard Roger.
Experimental test of bell's inequalities using time-varying analyzers.
Physical review letters, 49(25):1804, 1982.

[31] Charles H Bennett and Stephen J Wiesner.
Communication via one-and two-particle operators on einstein-podolsky-rosen states.
Physical review letters, 69(20):2881, 1992.

[32] Robert W Boyd.
Nonlinear optics.
Academic press, 2003.

[33] R_E Slusher, LW Hollberg, Bernard Yurke, JC Mertz, and JF Valley.
Observation of squeezed states generated by four-wave mixing in an optical cavity.
Physical Review Letters, 55(22):2409, 1985.

[34] Marco Fiorentino, Paul L Voss, Jay E Sharping, and Prem Kumar.
All-fiber photon-pair source for quantum communications.

Photonics Technology Letters, IEEE, 14(7):983–985, 2002.

[35] Chunle Xiong, Graham D Marshall, Alberto Peruzzo, Mirko Lobino, Alex S Clark, D-Y Choi, Steve J Madden, Chandra M Natarajan, Michael G Tanner, Robert H Hadfield, et al.
Generation of correlated photon pairs in a chalcogenide as2s3 waveguide.
Applied Physics Letters, 98(5):051101, 2011.

[36] X Zhang, I Jizan, J He, AS Clark, D-Y Choi, CJ Chae, BJ Eggleton, and C Xiong.
Enhancing the heralded single-photon rate from a silicon nanowire by time and wavelength division multiplexing pump pulses.
Optics letters, 40(11):2489–2492, 2015.

[37] Hiroki Takesue, Yasuhiro Tokura, Hiroshi Fukuda, Tai Tsuchizawa, Toshifumi Watanabe, Koji Yamada, and Sei-ichi Itabashi.
Entanglement generation using silicon wire waveguide.
Applied Physics Letters, 91(20), 2007.

[38] Damien Bonneau, Erman Engin, Kazuya Ohira, Nob Suzuki, Haruhiko Yoshida, Norio Iizuka, Mizunori Ezaki, Chandra M Natarajan, Michael G Tanner, Robert H Hadfield, et al.
Quantum interference and manipulation of entanglement in silicon wire waveguide quantum circuits.
New Journal of Physics, 14(4):045003, 2012.

[39] Joshua W Silverstone, Damien Bonneau, Kazuya Ohira, Nob Suzuki, Haruhiko Yoshida, Norio Iizuka, Mizunori Ezaki, Chandra M Natarajan, Michael G Tanner, Robert H Hadfield, et al.
On-chip quantum interference between silicon photon-pair sources.
Nature Photonics, 8(2):104–108, 2014.

[40] J Leuthold, C Koos, and W Freude.
Nonlinear silicon photonics.
Nature Photonics, 4(8):535–544, 2010.

[41] Jay E Sharping, Kim Fook Lee, Mark A Foster, Amy C Turner, Bradley S Schmidt, Michal Lipson, Alexander L Gaeta, and Prem Kumar.
Generation of correlated photons in nanoscale silicon waveguides.
Optics Express, 14(25):12388–12393, 2006.

[42] Ken-ichi Harada, Hiroki Takesue, Hiroshi Fukuda, Tai Tsuchizawa, Toshifumi Watanabe, Koji Yamada, Yasuhiro Tokura, and Sei-ichi Itabashi.
Generation of high-purity entangled photon pairs using silicon wire waveguide.
Optics express, 16(25):20368–20373, 2008.

[43] Stéphane Clemmen, K Phan Huy, Wim Bogaerts, Roel G Baets, Ph Emplit, and Serge Massar.
Continuous wave photon pair generation in silicon-on-insulator waveguides and ring resonators.
Optics express, 17(19):16558–16570, 2009.

[44] C Xiong, Christelle Monat, Alex S Clark, Christian Grillet, Graham D Marshall, MJ Steel, Juntao Li, Liam O,ÄôFaolain, Thomas F Krauss, John G Rarity, et al.
Slow-light enhanced correlated photon pair generation in a silicon photonic crystal waveguide.
Optics letters, 36(17):3413–3415, 2011.

[45] Chunle Xiong, Christelle Monat, Matthew J Collins, Laurent Tranchant, David Petiteau, Alex S Clark, Christian Grillet, Graham D Marshall, Michael J Steel, Juntao Li, et al.
Characteristics of correlated photon pairs generated in ultracompact silicon slow-light photonic crystal waveguides.
Selected Topics in Quantum Electronics, IEEE Journal of, 18(6):1676–1683, 2012.

[46] Erman Engin, Damien Bonneau, Chandra M Natarajan, Alex S Clark, MG Tanner, RH Hadfield, Sanders N Dorenbos, Val Zwiller, Kazuya Ohira, Nobuo Suzuki, et al.
Photon pair generation in a silicon micro-ring resonator with reverse bias enhancement.
Optics express, 21(23):27826–27834, 2013.

[47] Alex S Clark, Chad Husko, Matthew J Collins, Gaelle Lehoucq, Stéphane Xavier, Alfredo De Rossi, Sylvain Combrié, Chunle Xiong, and Benjamin J Eggleton.
Heralded single-photon source in a iii–v photonic crystal.
Optics letters, 38(5):649–651, 2013.

[48] Nobuyuki Matsuda, Hiroki Takesue, Kaoru Shimizu, Yasuhiro Tokura, Eiichi Kuramochi, and Masaya Notomi.

Slow light enhanced correlated photon pair generation in photonic-crystal coupled-resonator optical waveguides.
Optics express, 21(7):8596–8604, 2013.

[49] John S Bell.
On the einstein podolsky rosen paradox, 1964.

[50] Warren P Grice and Ian A Walmsley.
Spectral information and distinguishability in type-ii down-conversion with a broadband pump.
Physical Review A, 56(2):1627, 1997.

[51] Timothy E Keller and Morton H Rubin.
Theory of two-photon entanglement for spontaneous parametric down-conversion driven by a narrow pump pulse.
Physical Review A, 56(2):1534, 1997.

[52] Malte Avenhaus, Maria V Chekhova, Leonid A Krivitsky, Gerd Leuchs, and Christine Silberhorn.
Experimental verification of high spectral entanglement for pulsed waveguided spontaneous parametric down-conversion.
Physical Review A, 79(4):043836, 2009.

[53] Daniel FV James, Paul G Kwiat, William J Munro, and Andrew G White.
Measurement of qubits.
Physical Review A, 64(5):052312, 2001.

[54] I Jizan, AS Clark, LG Helt, MJ Collins, E Mägi, C Xiong, MJ Steel, and BJ Eggleton.
High-resolution measurement of spectral quantum correlations in the telecommunication band.
Optics Communications, 327:45–48, 2014.

[55] Thomas Gerrits, Martin J Stevens, Burm Baek, Brice Calkins, Adriana Lita, Scott Glancy, Emanuel Knill, Sae Woo Nam, Richard P Mirin, Robert H Hadfield, et al.
Generation of degenerate, factorizable, pulsed squeezed light at telecom wavelengths.
Optics express, 19(24):24434–24447, 2011.

[56] Christoph Söller, Benjamin Brecht, Peter J Mosley, Leyun Y Zang, Alexander Podlipensky, Nicolas Y Joly, P St J Russell, and Christine Silberhorn.
Bridging visible and telecom wavelengths with a single-mode broadband photon pair source.
Physical Review A, 81(3):031801, 2010.

[57] CK Law, IA Walmsley, and JH Eberly.
Continuous frequency entanglement: effective finite hilbert space and entropy control.
Physical Review Letters, 84(23):5304, 2000.

[58] Malte Avenhaus, Benjamin Brecht, Kaisa Laiho, and Christine Silberhorn.
Time-frequency quantum process tomography of parametric down-conversion.
arXiv preprint arXiv:1406.4252, 2014.

[59] Andreas Eckstein, Guillaume Boucher, Aristide Lemaître, Pascal Filloux, Ivan Favero, Giuseppe Leo, John E Sipe, Marco Liscidini, and Sara Ducci.
High-resolution spectral characterization of two photon states via classical measurements.
Laser & Photonics Reviews, 8(5):L76–L80, 2014.

[60] M. Halder, J. Fulconis, B. Cemlyn, A. Clark, C. Xiong, W. J. Wadsworth, and J. G. Rarity.
Nonclassical 2-photon interference with separate intrinsically narrowband fibre sources.
Opt. Express, 17(6):4670–4676, Mar 2009.

[61] O Alibart, J Fulconis, GKL Wong, SG Murdoch, WJ Wadsworth, and JG Rarity.
Photon pair generation using four-wave mixing in a microstructured fibre: theory versus experiment.
New Journal of Physics, 8(5):67, 2006.

[62] Malte Avenhaus, Andreas Eckstein, Peter J Mosley, and Christine Silberhorn.
Fiber-assisted single-photon spectrograph.
Optics letters, 34(18):2873–2875, 2009.

[63] Marco Liscidini and JE Sipe.
Stimulated emission tomography.
Physical review letters, 111(19):193602, 2013.

[64] Bin Fang, Offir Cohen, Marco Liscidini, John E Sipe, and Virginia O Lorenz.
Fast and highly resolved capture of the joint spectral density of photon pairs.
Optica, 1(5):281–284, 2014.

[65] Joshua W Silverstone, Raffaele Santagati, Damien Bonneau, Michael J Strain, Marc Sorel, Jeremy L O'Brien, and Mark G Thompson.
Qubit entanglement on a silicon photonic chip.
arXiv preprint arXiv:1410.8332, 2014.

[66] Nicolás Quesada and JE Sipe.
Effects of time ordering in quantum nonlinear optics.
Physical Review A, 90(6):063840, 2014.

[67] Chad A Husko, Alex S Clark, Matthew J Collins, Alfredo De Rossi, Sylvain Combrié, Gaëlle Lehoucq, Isabella H Rey, Thomas F Krauss, Chunle Xiong, and Benjamin J Eggleton.
Multi-photon absorption limits to heralded single photon sources.
Scientific reports, 3, 2013.

[68] Mirko Lobino, Dmitry Korystov, Connor Kupchak, Eden Figueroa, Barry C Sanders, and AI Lvovsky.
Complete characterization of quantum-optical processes.
Science, 322(5901):563–566, 2008.

[69] C McKinstrie and S Radic.
Phase-sensitive amplification in a fiber.
Optics express, 12(20):4973–4979, 2004.